Selection of the landing site in Isidis Planitia of Mars probe Beagle 2

J. C. Bridges,[1] A. M. Seabrook,[2,3] D. A. Rothery,[3] J. R. Kim,[4] C. T. Pillinger,[2] M. R. Sims,[5] M. P. Golombek,[6] T. Duxbury,[6] J. W. Head,[7] A. F. C. Haldemann,[6] K. L. Mitchell,[4,8] J.-P. Muller,[4] S. R. Lewis,[9] C. Moncrieff,[10] I. P. Wright,[2] M. M. Grady,[1] and J. G. Morley[4]

Received 12 November 2001; revised 15 February 2002; accepted 12 April 2002; published 4 January 2003.

[1] This paper describes selection and characterization of the landing site for the Mars 2004 Beagle 2 mission. The site is within Isidis Planitia between 10°–12°N, 266°–274°W, centered at 11.6°N, 269.5°W. This is at low elevation (−3600 to −3900 m MOLA), is flat (MOLA RMS slope = 0.57°), radar data suggest a smoother surface at decimeter to meter scales than the Pathfinder site and it has a moderate rock abundance (2–17%, mean 11%). In addition to this, Isidis shows evidence for concentration and remobilization of volatiles. In particular, the basin contains conical landforms. We favor models involving the formation of tuff cones during magma-ice interaction. Structures identified as dykes in MOC images may be remnants of magma conduits. The pattern of bulk thermal inertia in Isidis (higher values of 500 $Jm^{-2}s^{-0.5}K^{-1}$ around the SW-S-E margin decreasing toward the center and north) suggests that an influx of sediment spread from the Noachian areas around the southern half of the basin over the basin floor. The coarse, higher thermal inertia material was deposited closest to the sediment source. The variable state of erosion of the tuff cones suggests that they formed intermittently over a long period of time during Amazonian and possibly Hesperian epochs. Geologically recent resurfacing of Isidis has also occurred by aeolian processes, and this is shown by a deficit in impact craters <120 m diameter. The proportion of rocky material is predicted to be slightly less than the Viking and Pathfinder sites, but there will probably be more duricrust. *INDEX TERMS:* 5499 Planetology: Solid Surface Planets: General or miscellaneous; 6225 Planetology: Solar System Objects: Mars; *KEYWORDS:* Isidis, Beagle 2, Mars Lander, Mars Express

Citation: Bridges, J. C., et al., Selection of the landing site in Isidis Planitia of Mars probe Beagle 2, *J. Geophys. Res.*, *108*(E1), 5001, doi:10.1029/2001JE001820, 2003.

1. Introduction

[2] In this paper we outline why Isidis was selected from the potential landing areas as the Beagle 2 landing site. We also use available data to characterize its geological evolution including volcanic activity, topography, the pattern of rock and duricrust abundances as shown by maps of thermal inertia, aeolian activity and exobiological potential. Mars Orbiter Camera (MOC), Mars Orbiter Laser Altimeter (MOLA), Thermal Emission Spectrometer (TES) and pre-existing Viking images and Infra Red Thermal Mapping (IRTM) data have been examined. Earth-based radar observation data of Mars have also been used to gain information about the roughness of the site at decimeter to meter scales. The results for the chosen site in Isidis are presented here and are compared to those of the previous successful landers to give an indication of the nature of the land surface that can be expected during the Beagle 2 mission.

1.1. Beagle 2 Mission

[3] Beagle 2 is the small (60 kg including entry and landing systems) UK-led probe which is part of ESA's Mars Express Mission which will be launched in June 2003. Beagle 2 is named after H.M.S. Beagle, which is the ship Charles Darwin sailed upon between 1831 to 1836, during which voyage he made many of the observations that led him to write *Origin of Species*. Beagle 2 is Europe's first Mars Lander project. The Lander (~30 kg) will search for extinct life via isotopically fractionated organic material on and below (≤2 m) the surface using a mass spectrometer and stepped combustion-based system. It will also study the inorganic chemistry and mineralogy of the landing site with

[1]Department of Mineralogy, Natural History Museum, London, UK.
[2]PSSRI, Open University, Milton Keynes, UK.
[3]Department of Earth Sciences, Open University, Milton Keynes, UK.
[4]Department of Geomatic Engineering, University College London, London, UK.
[5]Department of Physics and Astronomy, University of Leicester, Leicester, UK.
[6]Jet Propulsion Laboratory, California Institute of Technology, Pasadena, California, USA.
[7]Department of Geological Science, Brown University, Providence, Rhode Island, USA.
[8]Environmental Science Department, Lancaster University, Lancaster, UK.
[9]AOPP, Department of Physics, Oxford University, Oxford, UK.
[10]Department of Zoology, Natural History Museum, London, UK.

0148-0227/03/2001JE001820$09.00

its suite of other instruments [*Sims et al.*, 2000]. An attempt will be made to search for extant life by looking for traces of methane within the atmosphere.

[4] The Beagle 2 instrument suite (~9 kg) consists of: a stereo camera pair with 24 filters including 11 narrow band mineralogy filters (440–1000 nm) distributed between the two cameras (these will also produce a 48° diagonal FOV with a close focusing distance of 0.6 m); a 4 color microscope with a resolution of ~8 μm for examination of rock and soil; an X-ray-Fluorescence Spectrometer for elemental composition; a Gamma-ray Mössbauer Spectrometer for determining iron oxidation and chemistry; a suite of environmental sensors measuring temperature, pressure, dust opacity, UV radiation; the Gas Analysis Package which can measure atmospheric gas composition as well as searching for organics via the stepped combustion method. Samples are collected by a variety of sample acquisition tools including the Mole. This is a self-burying penetrometer utilizing an internal hammer mechanism for propulsion. At its front end it carries a mechanism for acquiring a soil sample.

[5] Beagle 2 will be launched as part of Mars Express in June 2003. It will have a direct entry into the atmosphere at 5.6 kms^{-1} via a prograde approach and will land on Mars at the end of 2003. The probe will decelerate using radar altimetry, aerodynamic braking, parachutes and airbags, which will be jettisoned at appropriate points during the entry, descent and landing sequence which in total takes about 10 minutes. Mission duration is planned to be at least 180 Sols (Martian days). The Lander will be powered by solar arrays during the day and a Li-ion battery at night. Lander systems will be maintained within operating temperature limits using solar heat by day and heater power by night. The thermal design has been optimized for the chosen landing site and season. Data from the Lander will be relayed back to Earth via the Mars Express Orbiter and NASA's Mars Odyssey mission. The Lander will be controlled from a UK-based operations center.

1.2. Landing Site Requirements

[6] The landing constraints for Beagle 2 were established to optimize the prospect of a successful landing and operation of the on-board power system. One important constraint, imposed by the parachute descent, is that the landing site must have elevation lower than the 6.1 mbar pressure datum. This was formerly defined as 0 km, but is equivalent to −1.6 km MOLA at $L_s = 0°$ [*Smith and Zuber*, 1998]. A safe landing requires a relatively obstacle-free land surface (defined as the majority of slopes <15° and little sign of widespread scarps, ridges etc.) within the calculated landing ellipses, most total rock abundances 5–15% (corresponding to 5% of the surface covered by rocks of >0.2 m height), moderate thermal inertia (which relates to rock and dust abundance). Considerations of solar power dictate that the site must be close to the equator. Safe wind speeds during the parachute landing process are ≤ 15 ms^{-1} particularly within the last 100 m of descent. The primary data for atmospheric, wind and surface temperature modeling were derived from the European Mars Climate Database [*Lewis et al.*, 1999]. The approach is similar in terms of constraints to that used for the Pathfinder mission [*Golombek et al.*, 1997a].

[7] The landing ellipse sizes and orientations were calculated from Monte Carlo simulations, prepared by the Mars Express investigation team. The ellipse geometry depends upon the flight path angle (fpa) of Beagle 2 as it enters the Martian atmosphere. An initial set of 3 landing ellipses was used in establishing the area within which the final ellipse would be situated. Of these 3 ellipses, the largest, with the smallest fpa considered by us (15°), is 495 km × 93 km with a 77.6° clockwise from north azimuth. This covers an area of 35 000 km^2. A smaller ellipse - used for selection of the landing coordinates after all of the data had been collected around the area of the initial ellipses - is 174 km × 106 km with a 74.9° azimuth. This ellipse has an area of 14 500 km^2. Ellipse dimensions and orientations are summarized in Table 1. It is possible that by the time of landing the navigational errors will have been modeled to an accuracy allowing this ellipse size to be reduced further. In this paper longitude is quoted as degrees west in accordance with the planetographic system commonly used for Mars. However, more accurate aerocentric longitude and latitude coordinates on MOLA Digital Elevation Models are now available and these were used for selection of the site (e.g., 270.0°W as quoted in this paper is equivalent to 90.0°E aerocentric longitude for the landing site). Both coordinate systems are used in our figures.

[8] The zone of possible latitudes, consistent with sufficient sunlight for the solar arrays to operate during the northern hemisphere's mid winter to early spring (the projected duration of the lander's operations is from L_s = 322° to 53°), lies between 12°S and 12°N latitude. Most dust storm activity on Mars occurs before this season, in late southern spring. For instance, *Smith et al.* [2001b] used Thermal Emission Spectroscopy data to describe large equatorial dust storms between L_s 225° and 245° and a general decrease in dust storm activity by L_s = 345°.

2. Potential Landing Areas From Which Isidis Was Selected

[9] In this section we describe the areas on Mars that were assessed as possible landing areas in terms of their suitability for the scientific aims of the mission and where the terrain favors a safe landing. The main potential landing region extends for 7000 km from Amazonis Planitia (160°W), westward through the Elysium basin centered at 220°W to the Isidis basin at 270°W (Figure 1). This region mainly lies to the north of the scarp that divides the lowlands and highlands near the equator although the Isidis basin postdates and overlies this dichotomy boundary. MOLA elevation across the region varies from −1 to −4 km.

[10] Other areas of low elevation within the viable range of latitudes include Ganges Chasma (45°W, 10°S) and Simud Valles (37°W, 6°N) south of the Chryse channels, but these areas were not free of obstacles within the required initial landing ellipse dimensions and so are not considered here. Sinus Meridiani around 0°W, 2°S has attracted interest as a site for future landers because of the probable presence of haematite deposits [*Christensen et al.*, 2000]. However, most of this area lies at or above −1.6 km MOLA so it was not considered in the final selection of sites for Beagle 2.

[11] Much of Elysium and Amazonis Planitia are covered by lava flows which could be as young as 10 Ma [*Hartmann*

Table 1. Landing Ellipse Dimensions and Azimuth for Different Flight Path Angles[a]

	fpa			
	15°	18°	20°	Final (16.5°)
Ellipse dimension, km	495 × 94	387 × 94	328 × 94	174 × 106
Azimuth	77.6°	70.4°	63.4°	74.9°

[a]Here, fpa, flight path angle. The ellipses' dimensions are for 3 standard deviations (s.d.), corresponding to 99% probability ellipses. One and 2 s.d. ellipses would be one third and two thirds of the dimensions shown in the table, corresponding to 39% and 86.5% probability ellipses. The largest ellipses were used for the initial selection of the landing area and the smallest ellipse, which was calculated afterwards, for the final selection of the coordinates aimed at. Azimuth (clockwise from north) is of ellipse major axis. Pathfinder and Viking landing ellipses were 200 × 100 km with 67.5° (clockwise from north) azimuth. It is possible that at the time of the Beagle 2 landing, improved navigational accuracy will lead to a smaller landing ellipse.

and Berman, 2000]. This is the smoothest part of the northern lowlands at the kilometer and hundred meter scale [e.g., *Kreslavsky and Head*, 2000]. However, pristine mare-like lava flows are likely to have rough surfaces at the meter-scale and so would not be suitable for Beagle 2. The Cerberus Plains (in parts of SE Elysium, 3°N, 230°W to 10°S, 120°W) contain, in addition to young lava flows, the Medusae Fossae Formation (Am in the geological unit notation of *Tanaka et al.* [1992]), large sand sheets, and some flood channels smaller than the landing ellipse size as at 18°N, 175°W [e.g., *McEwen et al.*, 2001]. The Medusae Fossae Formation - which has the greatest areal extent of the different mapped geological units in the region - is an erosional terrain the origin of which is highly debated (see summary of hypotheses by *Zimbelmann et al.* [1997, 1999] and *Sakimoto et al.* [1999]).

[12] An area of Amazonian Smooth Plains (Aps) is present between 190–200°W, 0°–10°N. However, inspection of narrow angle MOC images reveals the presence of kilometer-long scarp slopes and an uneven land surface on the meter to tens of meters scale. Some images within this Aps outcrop also show eroded land surfaces with dissected lava flows or strata visible. This rugged land surface is not suitable for Beagle 2 and so was not considered further.

[13] *Parker et al.* [1993] proposed that contacts that they mapped along the margins of the northern lowlands represented shorelines from previous oceans formed from the Hesperian outflow channels. According to their mapping, these deposits closely correspond to the margins of the Vastitas Borealis Formation, and the arrangement of the contacts led to their interpretation that the northern lowlands (including the Isidis Basin) was flooded by standing bodies of water at this time. If such bodies of water indeed existed in the Hesperian, they apparently disappeared by the early Amazonian [*Head et al.*, 1999; *Ivanov and Head*, 2001]. *Kreslavsky and Head* [2002] have suggested that the Vastitas Borealis Formation (such as the region within Isidis) may represent the sedimentary residue remaining from frozen outflow channel effluents that subsequently sublimed.

2.1. Thermal Inertia and Albedo Data on Potential Landing Areas

[14] Remote data on thermal inertia (TI) and albedo were also useful in making the choice of landing site from within the potential landing region by providing information about rock and dust distribution. Thermal inertia data were used to predict rock abundances accurately at the Viking and Pathfinder sites prior to those landings [e.g., *Golombek et al.*, 1999].

[15] Much of the Elysium-Amazonis Planitia region has moderate TES thermal inertia values <330 $Jm^{-2}s^{-0.5}K^{-1}$ [*Mellon et al.*, 2000]. The Mars average TI is approximately 250 $Jm^{-2}s^{-0.5}K^{-1}$. Some areas from 150°W–180°W, 0–

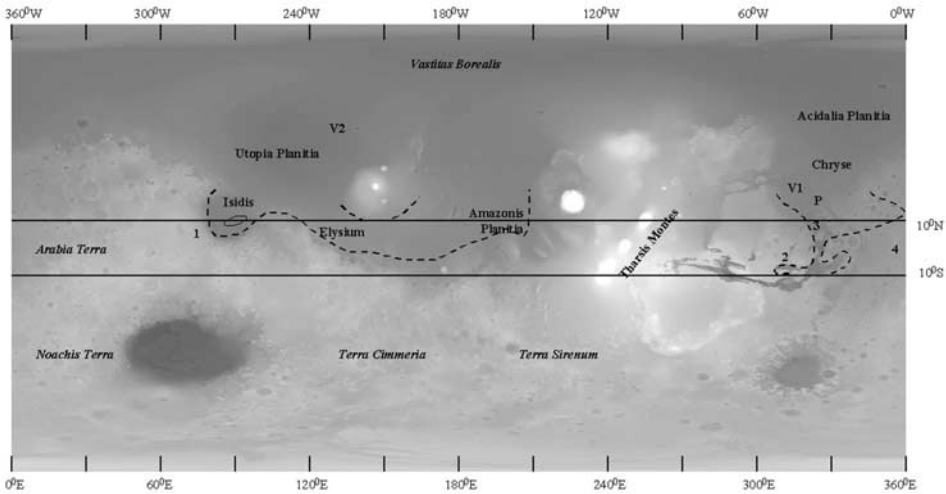

Figure 1. Map of Mars (MOLA 1/64th DEM-based topographic shaded relief map) showing location of potential landing sites for Beagle 2. Dashed line is position of −1.6 km MOLA contour (approximately equivalent to MDIM1 0 km pressure datum). The latitude lines at 12°N and 12°S show the approximate limits within which the Lander is designed to function. V1, Viking 1 site in outflow plain within Chryse Planitia; V2, Viking 2 in Utopia Planitia; P, Pathfinder in Ares Vallis. The Beagle 2 landing ellipse (495 km length) is shown in Isidis basin. Other numbered localities mentioned in this paper are 1, Syrtis Major; 2, Ganges Chasma; 3, Simud Valles; 4, Sinus Meridiani. Data from MOLA Science Experiment Team.

12°N have very low TI values (<75 $Jm^{-2}s^{-0.5}K^{-1}$). This includes the Medusae Fossae Formation and much of Amazonis Planitia, although there is no direct correlation between the geological map units and the areas with low TI. The low TI values are consistent with a coating of dust (from a few cm to a meter thickness), which has led to the high albedos of these areas [*Christensen and Moore*, 1992]. This dust coating is not thick enough to mask the underlying landforms in MOC images but might partially cover the solar panels if it was remobilized during the mission.

[16] Most of the remaining parts of the region have both intermediate TI values (e.g., 120–300 $Jm^{-2}s^{-0.5}K^{-1}$) suggesting slightly less rocky surfaces than the Pathfinder and Viking 1 landing sites in the Chryse region, which have TI values of 380 and 320 $Jm^{-2}s^{-0.5}K^{-1}$ TI [*Mellon et al.*, 2000]. Rock abundances are calculated from bulk thermal inertia data assuming the ground surface is composed of a rock component of high thermal inertia (e.g., 1250 $Jm^{-2}s^{-0.5}K^{-1}$) with the remainder being allocated to the fine component thermal inertia. See *Christensen* [1986], *Mellon et al.* [2000], and *Golombek et al.* [2001] for models and TI values assumed for rock and fine component end-members.

[17] However, the TI modeling does more than just give information about rock fragments (≥0.10 m diameter) on the surface. Bulk thermal inertia measurements are often dominated by the fine component TI, and *Mellon et al.* [2000] and *Jakosky and Christensen* [1986] noted that high thermal inertias recorded by TES, in some areas of Mars, could indicate the presence of cemented duricrusts or sand, particularly intracrater dunes. On the basis of TI modeling, *Mellon et al.* [2000] divided the Martian surface into 3 main units: unit A with low TI and high albedo (e.g., Arabia and Tharsis), B with high TI and low albedo (e.g., the ancient highlands between 30°S–60°S), and C with intermediate TI and albedo values (Viking 1,2, much of the lowland equatorial region between 200°E and 90°E including the northern half of Isidis). A fourth unit, D, with high TI did not fit into these 3 main categories (e.g., the Pathfinder site in Ares Vallis and the southern half of Isidis). The intermediate physical properties of C could not be explained solely through a gradational change in the distribution of dust between dust-rich Type-A surfaces and dust-poor Type-B surfaces because the frequency plots of TI readings of the Martian surface do not show a gradational change between low and high TI values. Instead *Mellon et al.* [2000] suggested that it marked the presence of duricrusts, such as those identified at the Viking and Pathfinder sites. A type C site with a mixture of rock and duricrust and soil with a limited covering of dust that could be remobilized is suitable for the design of Beagle 2 and its sampling instrumentation.

[18] As a result of these remote data considerations and the nature of the land surfaces as outlined in the previous section, the Isidis basin (with predicted rock abundances within the acceptable range and a relatively smooth land surface) was selected for the Beagle 2 landing site and detailed characterization.

3. Characterization of the Isidis Surface

3.1. Basin Structure and Topography

[19] The northern lowlands are characterized by relatively thinner crust than the ancient highlands (averaging about 35–40 km [*Zuber et al.*, 2000]), and consist of four topographic basins, North Polar, Chryse, Isidis and Utopia. Isidis and Utopia are clearly of impact origin and Chryse may also be of impact origin, the impact events occurring within the Noachian Period [e.g., *Schultz and Frey*, 1990; *McGill*, 1989; *Head et al.*, 2002]. Only Isidis lies across the range of latitude 12°S to 12°N. It is not clear how the overall crustal division between the lowlands and ancient highlands originated. For instance, an impact origin would have required the disposal of an unfeasibly large volume of crust across the rest of Mars [*McGill and Dimitrou*, 1990]. *Zuber et al.* [2000] explore internal mechanisms. There is evidence of a Noachian surface underlying the near-surface deposits [e.g., *Frey et al.*, 2001] and the northern lowlands experienced extensive volcanism during the early Hesperian [e.g., *Head et al.*, 2002]. The Isidis and Utopia basins have large positive mass anomalies [*Smith et al.*, 1999] and Isidis in particular has the largest anomaly within 30° north or south of the equator [e.g., *Phillips and Saunders*, 1975]. *Zuber et al.* [2000] and others have interpreted the combined gravity and topography data to reflect basin infill by sediments or lavas, and/or, thinning of the crust underlying the basin.

[20] *Head et al.* [2002] showed that compressional tectonic features (wrinkle ridges), up to hundreds of km long, appear to form a concentric pattern around the Tharsis dome, and distinct patterns within the Isidis and Utopia basins and elsewhere within the northern lowlands. These wrinkle ridges [*Chicarro et al.*, 1985] are markedly similar to those of the lunar maria.

[21] The stratigraphic relationship of formations that are contemporaneous with or postdate the Early Hesperian (Hr) plains and the superposed wrinkle ridges in the northern lowlands is seen within the Isidis basin and is as follows [*Greeley and Guest*, 1987]: 1. The Upper Hesperian Vastitas Borealis Formation (Hvr), exposed in a broad arc in the central and western floor of the Isidis basin (Figure 2). This is the ridged member, consisting of concentric low ridges about 1–2 km wide. 2. Amazonian Smooth Plains (Aps), which form regions of lightly cratered, flat featureless plains interpreted by *Greeley and Guest* to be of diverse origin, with many units being of aeolian origin. Aps is exposed around the margins of the basin floor and in the northeast part of the basin interior. These sediments were deposited predominantly on top of the Hr lava flows partially obscuring the wrinkle ridge topography, as at the Viking 1 site in Chryse Planitia. *Grizaffi and Schultz* [1989] and *Tanaka et al.* [2000] suggested that Isidis had been covered by a layer of volatile-rich sediment at one stage in its history and this question of the presence of sediments is considered further in the light of MOC and MOLA data in later sections.

[22] The concentric structure of the Isidis Basin (Figure 2) has been described by *Frey et al.* [2000]. They showed that there are three structural zones: an inner 1100 km ring enclosing the Aps and Hvr plains material from 2–22°N and 262–282°W (''Inner Deposits'' and containing the Beagle ellipses); a 1500 km ''main ring'' which in the south-west is covered by the Syrtis Major shield volcano lavas and contains ancient highland rim material to the south from 0–25°N and 260–285°W; a third, 1900 km outer margin ring from 3°S–27°N, 258–268°W. The main ring occupies a broad depression and this is shown by a break in slope in the Syrtis Major lava flows which

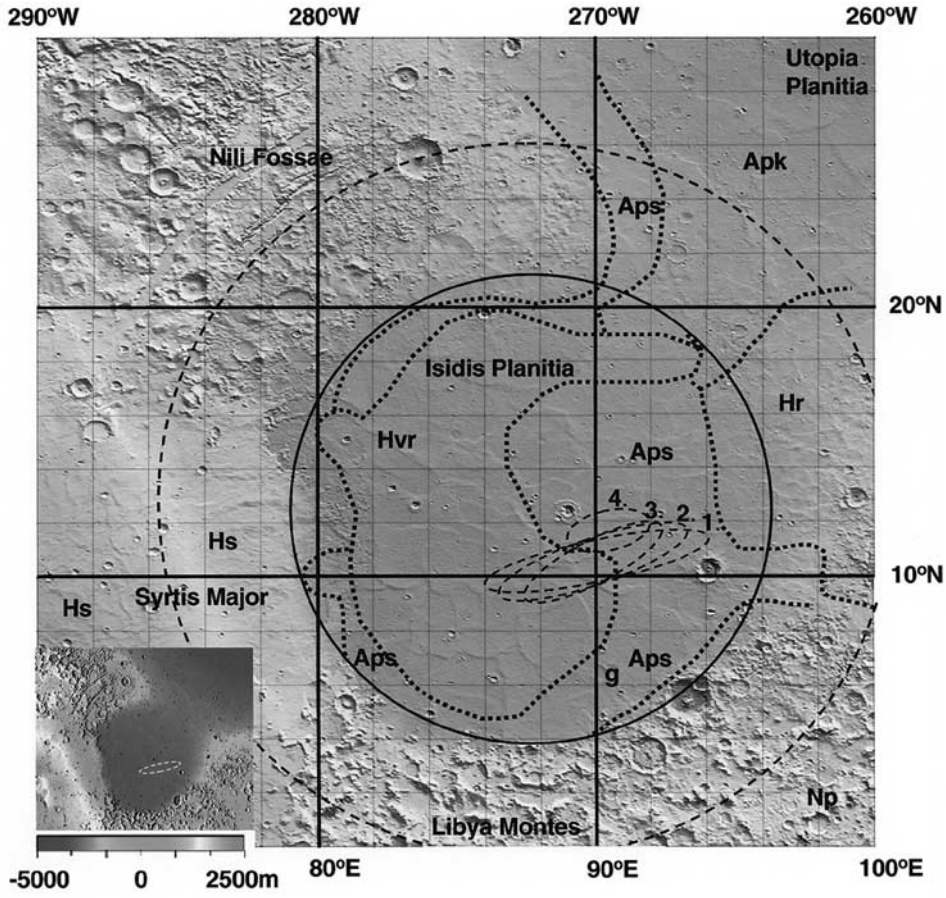

Figure 2. Location of Beagle initial landing ellipses (maximum length 495 km) and final landing ellipse (maximum length 174 km) within Isidis Planitia. Diagram from 1/64th MOLA DEM. 1, 2, 3, 4 Beagle landing ellipses for flight path angles of 15°, 18°, 20°, and final landing ellipse (Table 1). The 1500 km diameter "Main Ring" and the 1100 km Inner Ring [*Frey et al.*, 2000] are shown. Aps, Amazonian Smooth Plains Deposits; Apk, Amazonian Knobby Plains Unit; Hr, Hesperian Ridged Plains; Hvr, Ridged Plains member of Vastitas Borealis Formation; Hs, Syrtis Major Formation; Np, undivided Noachian Plateau sequences [*Greeley and Guest*, 1987]. Dotted lines are the boundaries between these units. G indicates two of the ghost craters, partially filled by Amazonian sediment, in the south of the basin. Inset shows the MOLA 1/64th DEM of the Isidis basin with elevation scale. Data from MOLA Science Experiment Team.

partially overlap the basin [*Frey et al.*, 2000]. The overall elevation decrease from outer rim to basin floor is 5000 m. The Isidis basin is probably underlain by lavas, which is consistent with the wrinkle ridge topography. *Solomon and Head* [1980] suggested that the circumferential grabens, within the NW outer margin of Isidis (Figure 2), of which Nili Fossae is the largest, within the NW outer margin of Isidis (Figure 2) are the result of lavas downloading the lithosphere. Other graben are located to the SE of the inner ring and are overlain by the Aps deposits. The Isidis basin is also slightly tilted down toward the SW with a drop in elevation of 300 m across the inner ring from NE to SW. *Tanaka et al.* [2000] suggested that this tilt was the result of isostatic adjustment due to sedimentary loading in the Utopia basin to the NE. Within this overall regional slope trend, elevated zones <6 km wide correspond to the underlying wrinkle ridges of the Hesperian Ridged Plains member (Hr).

[23] The eastern margin of Syrtis Major is fractured and degraded creating a chaotic-like terrain leading into the Isidis basin. *Tanaka et al.* [2000] proposed that the Isidis plains experienced a catastrophic influx of volatile-rich mud from this region. They also suggested that the Inner Plains deposits within the central part of the basin floor, corresponding to the Aps and Hvr deposits of *Greeley and Guest* [1987], are in fact of the same age and derived from the breakup of the Syrtis Major shield. As part of this model the cones which characterize Isidis were suggested to be a result of the release of volatiles that had been trapped within the units at the time of their deposition. A later section reviews the evidence for cone origin.

3.2. Thermal Inertia and Albedo Measurements of Isidis

[24] We have used TES thermal inertia (TI) data from *Mellon et al.* [2000] to construct a high resolution map of

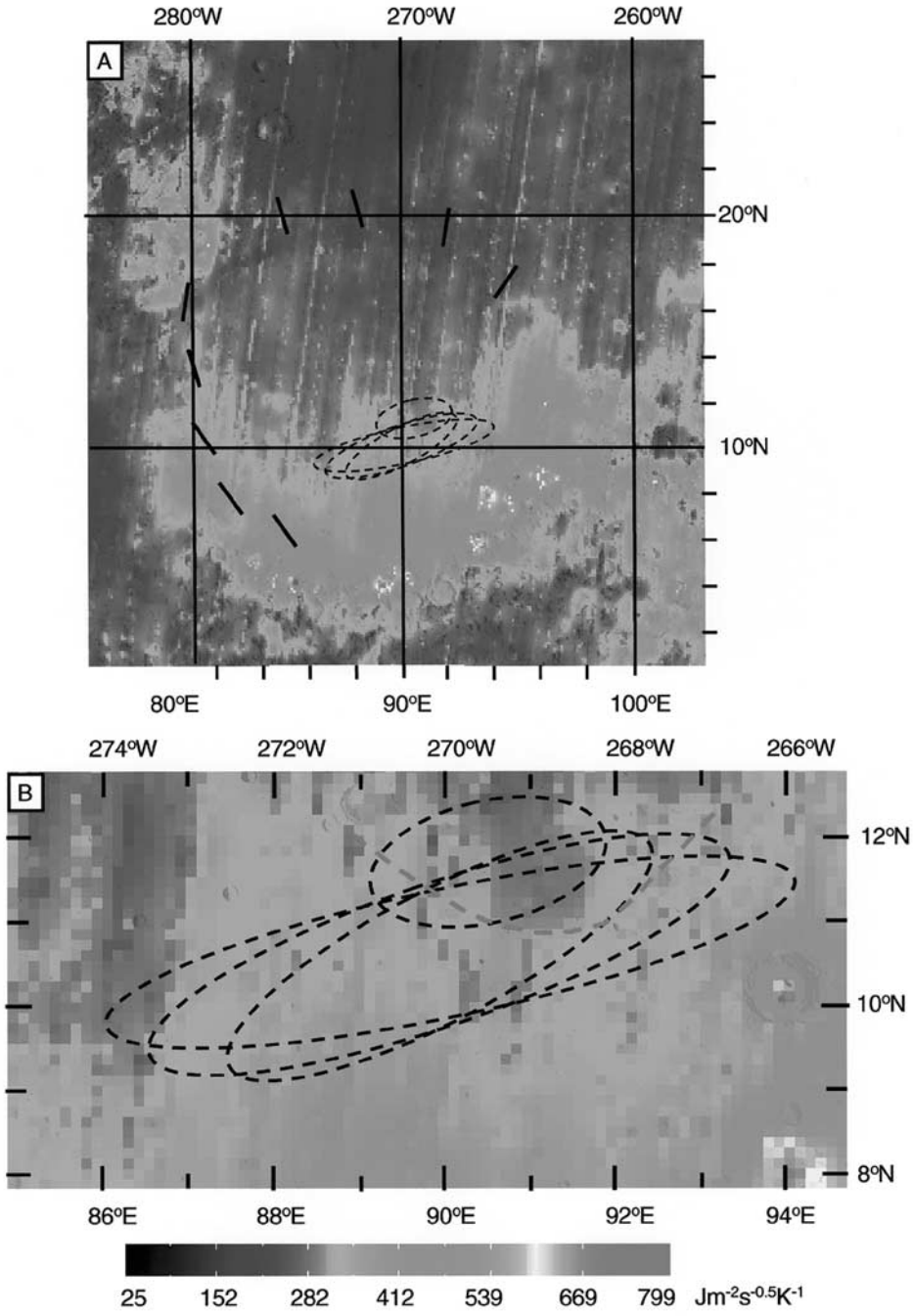

Figure 3. (a) Bulk Thermal Inertia maps of Isidis Planitia and (b) area around landing ellipses using uninterpolated data from *Mellon et al*. [2001], with a resolution of 8 pixels per degree. Landing ellipses shown as for Figure 2. Dashed line in Figure 3b is the contour dividing areas with predicted wind speeds at 900 m elevation >12 ms^{-1} to the south from lesser speeds to the north. The short trend lines of cones [*Grizzaffi and Schultz*, 1989] are also shown around the inner margin of the inner ring.

Isidis and the area covered by the landing ellipse (Figure 3, Table 2). This shows that the lowest bulk TI values <300 $Jm^{-2}s^{-0.5}K^{-1}$ are found to the north and west of the basin, whereas TI in most of the basin interior, including across the landing ellipses is 300–400 $Jm^{-2}s^{-0.5}K^{-1}$. The highest values, >500 $Jm^{-2}s^{-0.5}K^{-1}$, are found toward the SW-S-E margins of the basin. This partially coincides with the outcrop of the Aps formation which mantles much of the margin of the basin floor (Figure 2). There is some variation between the Viking IRTM and Mars Orbiter TES data sets for thermal inertia (Table 2). This may be because the IRTM data set has lower pixel resolution and also because different models have been used for calculating surface thermal inertias. The predicted rock abundances are from *Christensen* [1986] and these were calculated from IRTM thermal band differencing. The landing ellipses' rock

Table 2. Summary of Remote Data in the Region Enclosing Beagle 2 Landing Area and the Pathfinder and Viking 1 Landing Sites[a]

	Beagle 2, Isidis	Pathfinder, Ares Vallis, 1997	Viking 1, 1976
Lat., Long.	11.6°N, 269.5°W	19.5°N, 32.8°W	22.4°N, 48.0°W
Elevation [MOLA]	−3.6 to −3.8 km	−3.7 km	−3.6 km
Geology	Aps, plain	Hch, outflow plain	Hch, outflow plain
MOLA slopes rms, median[b]	0.57°, 0.3°	0.3°	0.2°
GSSR radar (rms) slopes[c]	2.4° ± 0.9°, 3.2° ± 1.3°	5.4° ± 1.1°	
TES bulk TI mean, range[d]	355; 283–675	418; 356–542	320; 277–375
TES albedo mean, range[d]	0.26; 0.25–0.27	0.22; 0.19–0.24	0.26; 0.23–0.27
Red/violet reflect. ratio[e]	2.7	2.25	2.6
IRTM fine TI mean, range[e]	366, 272–422	344	289
IRTM bulk TI mean, range[e]	405, 380–489	403–542	336–357
IRTM albedo[e]	0.23; 0.22–0.25	0.19–0.23	0.23–0.25
IRTM rock abundance[e]	11%; 2–17% range	16%	15%

[a]Beagle 2 ellipse used is one centered at 11.6°N, 269.5°W. TES, Thermal Emission Spectrometer (Mars Global Surveyor); TI, thermal inertia; IRTM, Infrared Thermal Mapper (Viking Orbiters). Aps, Amazonian Smooth Plains Deposit; Hch, Hercynian Channel Deposits.

[b]Slope values from *Aharonson et al*. [1989] and (for Isidis) this study. RMS slopes are larger than median slopes because they are influenced by a small number of greater slopes in the tail of the slope distribution [*Kreslavsky and Head*, 1999; *Aharonson et al.*, 2001].

[c]Goldstone Solar System Radar (GSSR) RMS slopes (this study) with standard deviations of the unweighted means. The two values for Isidis are those over Aps and Hvr rock units respectively (see Table 3).

[d]TES TI data from *Mellon et al.* [2000]. Albedo kindly provided in advance of publication by P. Christensen.

[e]An integrated digital IRTM data set kindly provided by P. Christensen and see sources in *Golombek et al.* [1997a].

abundances are 2–17% with most of the higher part of this range in the SW half of the ellipses where the TES TI exceeds 300 $Jm^{-2}s^{-0.5}K^{-1}$. The average rock abundance in the region of the landing ellipse (265–274°W, 9–12°N) is 11% and the highest rock abundances (28%) are found over the large craters outside the landing ellipses (e.g., at 10°N, 266°W). Within the final landing ellipse the rock abundances vary from 0–15%.

[25] Comprehensive albedo measurements of Mars from the Viking Orbiter IRTM were reported for 1977 by *Pleskot and Miner* [1981]. The albedo in Isidis was found to vary considerably through the year, the highest values 0.20–0.30 occurring from L_s 337 to 0° (northern winter, southern summer) when dust was settling from the atmosphere after a global dust storm. From L_s 46 to 60° (early northern spring) when the effects of the dust storm had diminished, the albedo in Isidis was 0.20–0.25. This is taken to be representative of the normal Isidis albedo. It is similar to the albedos of the Viking 1 and Pathfinder sites (0.20–0.25) and slightly lower than that of the Viking 2 site (0.25–0.30) when measured at the same season. It is also similar to the TES albedo measurements in the region of the Beagle 2 landing ellipses which are 0.25–0.27 (Table 2). This moderate albedo (e.g., compared with much of Tharsis and Arabia Terra which have higher albedos, and the adjacent Syrtis Major basin which is one of the darkest regions on Mars) is consistent with a partial covering, $\geq$ μm thick, of reflective dust. It has been demonstrated that dust landed on Pathfinder's solar arrays at the rate of 5–15 μm/yr [*Landis and Jenkins*, 2000]. Much of this dust influx onto the Isidis rocks and soil will be remobilized, which is consistent with variation in the measured albedo between seasons as described above.

[26] The higher fine component thermal inertia of the Isidis site compared with the Viking and Mars Pathfinder landing sites argues that there is less dust at Isidis relative to that found at the other three sites.

[27] The albedo and TI measurements of Isidis are closest to the characteristics of the Unit C mapped on Mars by *Mellon et al.* [2000], although the range of Isidis TI values extends to greater values in the southern part of the landing ellipse and Mellon et al. left that part of Isidis in an uncertain category (Unit D). Higher TI values in the south of the area do not correlate with the presence of sand dunes as MOC images reveal their presence across the entire basin, therefore the high TI component in the bulk measurements is unlikely to be dominated by sand-sized particles. The rock ($\geq$0.10 m) abundance model of *Christensen* [1986] proved accurate for Ares Vallis [*Golombek et al.*, 1997b] so there can be confidence that it will also be applicable to Isidis which has similar albedo and TI characteristics.

[28] The relatively high TI values of the landing area probably represent a mixture of rock (comprising up to 17% of the ground surface) and duricrust surrounded by finer grains and partially covered by reflective dust. The presence of duricrust over much of the landing ellipse surface is suggested by the fine component TI, which is higher for Isidis than the other successful landing sites [*Mellon et al.*, 2001]. In addition to the duricrust coverage, using the rock abundance curves of *Golombek et al.* [1999] and *Golombek and Rapp* [1997] for an average rock abundance of ~15% suggests that 6% of the Isidis landing site surface is covered by rocks of >0.1 m height, 5% rocks >0.2 m height, and 10% of the surface is covered by rocks >0.1 m diameter. The height and width values are based on data sets derived from Viking Lander images [*Golombek and Rapp*, 1997].

[29] If it is assumed that rock abundances increase with proximity to their sediment source, then it is likely that the highest TI regions in the Isidis basin (reflecting greater rock abundances) are closest to the sediment source for the rocky material on the Isidis plains. As the highest TI values are concentrated around the southern margin of Isidis, it is likely that the Isidis rocks are debris brought in from the Noachian highland areas to the south of the basin. The pattern of TI is not consistent with the majority of rocky material being brought in from Syrtis Major as suggested by *Tanaka et al.* [2000].

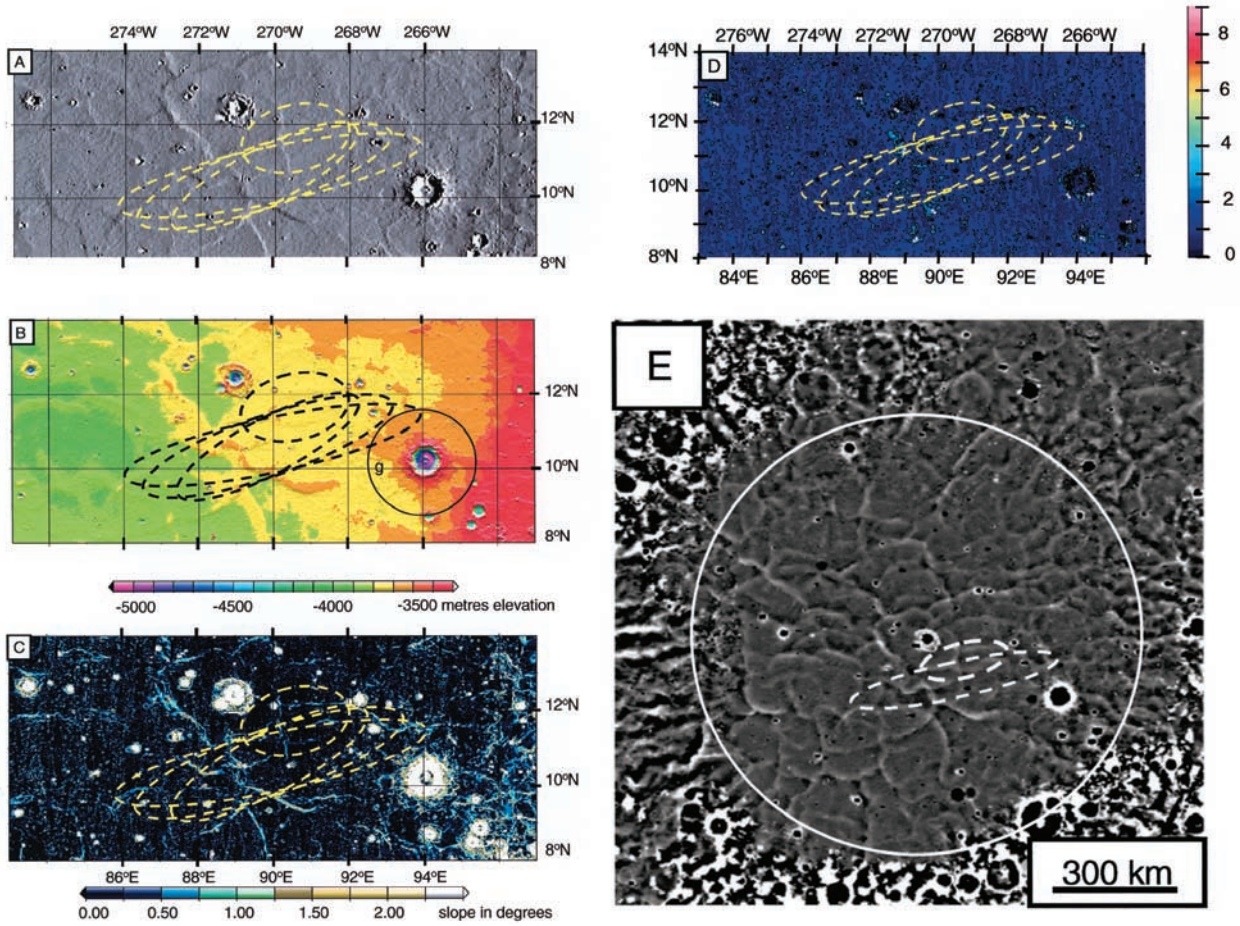

Figure 4. Topographic maps and slopes of Isidis using gridded 1/64th DEM for Figures 4a and 4b and 1/128th DEM for Figure 4c. Data from MOLA Science Investigation Team. Landing ellipses for three flight path angles (fpa) and final landing ellipse are shown in Figures 4a–4d. (a) Shaded relief map showing subdued wrinkle ridges across the landing ellipses. (b) Topographic map. There is a gentle slope from −3600 m to −3900 m from NE to SW within the landing ellipse areas. The area of higher topography running ENE-WSW is the surface expression of a wrinkle ridge, ≤150 m above the surrounding area. The black circle marks the possible extent of ejecta from the 60 km diameter crater in its center. This can be seen to intersect the NE corner (450 km^2) of the 15° fpa ellipse. G is partially buried "ghost" crater. (c) Calculated slopes between MOLA points. The slopes were derived from MOLA gridded DEM of 1/128th resolution. Original DEM was made with a linear semi-variogram model calculation and kriging in 64 arrays. All MOLA spots were crossover corrected before kriging. Noise tracks were removed and then E-W slope and N-S slope were calculated by total slope = sqrt((E-W slope)*(E-W slope) + (N-S slope)*(N-S slope)) using arc length. The root mean square (rms) values of these are 0.38° and 0.34°, giving a combined NS and EW RMS slope of 0.57°, total slope = sqrt(NS*NS + EW*EW). The generally flat nature of the region is evident and the calculated average RMS slope is 0.57°. The wrinkle ridge and impact craters are the only areas at this scale with slopes >2.5°. (d) Vertical roughness (rms) map derived from MOLA pulse width data, with the scale showing relief within individual ∼150 m diameter MOLA backscattered laser shots on the Martian surface. Shot to shot slopes removed as described by *Garvin et al.* [1999] and *Smith et al.* [2001a]. The prominent wrinkle ridge is apparent as an area with relief >4 m, but otherwise this figure is consistent with Figures 4a–4c in showing the generally flat nature of the Beagle 2 landing area. (e) Detrended topographic map of Isidis Planitia (regional slope removed). The map is centered at 13°N, 272°W; north is at the top; map projection is simple cylindrical. Filter core radius used is 50 km. The map shows Isidis to be underlain by a wrinkle ridge basement similar to that of lunar mare. See *Head et al.* [2002] for details.

Table 3. Isidis GSSR Delay-Doppler Radar Data and Hagfors Model Analysis[a]

Radar Tracks Across Isidis	Latitude, °N	Longitude Coverage, °W Start	End
1992/1993 Opposition			
21 January 1993	5.11°	234.11°	277.19°
23 January 1993	4.86°	183.33°	279.79°
1994/1995 Opposition			
31 December 1994	21.56°	265.95°	332.82°
8 February 1995	18.87°	210.82°	330.68°
11 March 1995	16.84°	268.02°	336.84°
18 March 1995	16.83°	204.75°	315.36°
Radar Data Summary	**Samples**	**Reflectivity**	**RMS slopes**
Geologic Unit[b,c]		ρ_0	θ_{rms}
Apk, knobby plains material	119	0.04 ± 0.03	2.9° ± 1.3°
Aps, smooth plains material in northern plains assemblage	288	0.04 ± 0.02	3.2° ± 1.3°
Hnu, undivided material in plateau and high plains assemblage	26	0.01 ± 0.01	5.5° ± 2.0°
Hvr, ridged member of northern plains assemblage	189	0.05 ± 0.02	2.4° ± 0.9°
Hr, ridged plains material	42	0.07 ± 0.02	5.1° ± 1.1°
Hs, Syrtis Major formation	16	0.06 ± 0.01	2.6° ± 0.3°
Nplh, hilly unit in plateau sequence	53	0.04 ± 0.02	5.5° ± 2.0°
Npl2, subdued cratered unit in plateau sequence	8	0.02 ± 0.01	6.3° ± 2.6°
Npld, dissected unit in plateau sequence	52	0.03 ± 0.02	4.6° ± 1.7°
Nple, etched unit in plateau sequence	6	0.05 ± 0.01	4.3° ± 0.5°
Mars Pathfinder Comparison	**Samples**	**Reflectivity**	**RMS Slopes**
Geologic Unit[d]		ρ_0	θ_{rms}
Hchp, floodplain materials	174	0.04 ± 0.03	4.7° ± 1.8°
Hch, older channel materials	256	0.04 ± 0.02	4.7° ± 1.6°
Landing site at 33.52°W, 19.28°	6	0.06 ± 0.01°	5.4° ± 1.1°

[a]The uncertainties are the standard deviations of the unweighted means. Samples column gives number of analyses along the radar tracks. The Aps and Hvr rock units are present on the floor of the Isidis basin although none of the radar tracks overlaps the Beagle 2 landing ellipses.
[b]*Greeley and Guest* [1987].
[c]*Tanaka et al.* [1992].
[d]*Scott and Tanaka* [1986].

[30] The ratio of red/violet reflectivity for Isidis (2.6–3.0 [*Golombek et al.*, 1997a]) is slightly higher than that of the previous landing sites, suggesting the presence of a largely oxidized mineral assemblage e.g., containing ferrihydrite or haematite in the surface material. *McSween et al.* [1999] demonstrated for the Pathfinder results that high red/blue reflectance ratios correlated with SO_3 contents. Therefore the surface of Isidis is likely to consist of sulfur-bearing salts and ferric iron-rich minerals in duricrust and dust interspersed with rocks.

[31] The surface spectral signatures of Martian low albedo areas have been modeled using MGS thermal emission spectra, with basaltic regions apparently concentrated to the south of the crustal dichotomy and a more feldspar-rich, andesitic-like composition across much of the northern plains [*Bandfield et al.*, 2000]. However, as Isidis has a relatively high albedo, the spectral signature of igneous or sedimentary rocks that underlie the layer of duricrust and soil is unclear.

3.3. Wind Speed Modeling Across Isidis

[32] The results of both global atmospheric circulation studies of Mars under typical dust conditions [*Lewis et al.*, 1999] and complementary mesoscale wind modeling for L_s = 300–330° and 2pm local time across Isidis, suggest that the region within the initial landing ellipses to the south of about 10.5°N might have wind speeds at that time of Martian day which exceed the Beagle 2 safety limits. For this reason the final, smaller ellipse was centered at 11.6°N, 269.5°W, within an area of the landing site region predicted to have lower mean wind speeds, <12 ms^{-1} at 900 m elevation, and correspondingly low wind speeds within the final 100 m descent of the lander to the surface (Figure 3b).

3.4. Topography Across the Area of the Isidis Landing Ellipse

[33] Figures 4a–4c shows detailed MOLA-derived maps (data points on 1/64th degree and 1/128th degree gridded DEM) across the area of the initial and final landing ellipses in Isidis. Relatively higher ground, −3600 m, is at the ENE end of the ellipses and lower ground, −3900 m, occurs at the WSW ends. This drop in elevation gives a regional slope of ~0.03°. Similarly, within the final ellipse the drop in elevation is −3600 to −3800 m. The slopes across the area of the initial Isidis landing ellipses (Figure 4c, Table 2) were calculated from a MOLA DEM between data points in both north-south and east-west directions. The root mean square (rms) values of these are 0.38° and 0.34°, giving a combined NS and EW RMS slope of 0.57°. The combined median slope is 0.3°. This is comparable with median slopes of previous landing sites which are 0.3° at Pathfinder and 0.2° at Viking 1 [*Aharonson et al.*, 2001].

[34] Figures 2 and 4 show the slightly elevated ridges within the landing area that are superimposed upon this regional slope. The ridges correspond to wrinkle ridges described by *Head et al.* [2001] that are present across much of the northern plains. In Isidis they are ≤150 m above the surrounding plains. The most prominent ridge is WNW-ESE trending and lies across the center of the initial landing ellipses. In order to check the slopes associated

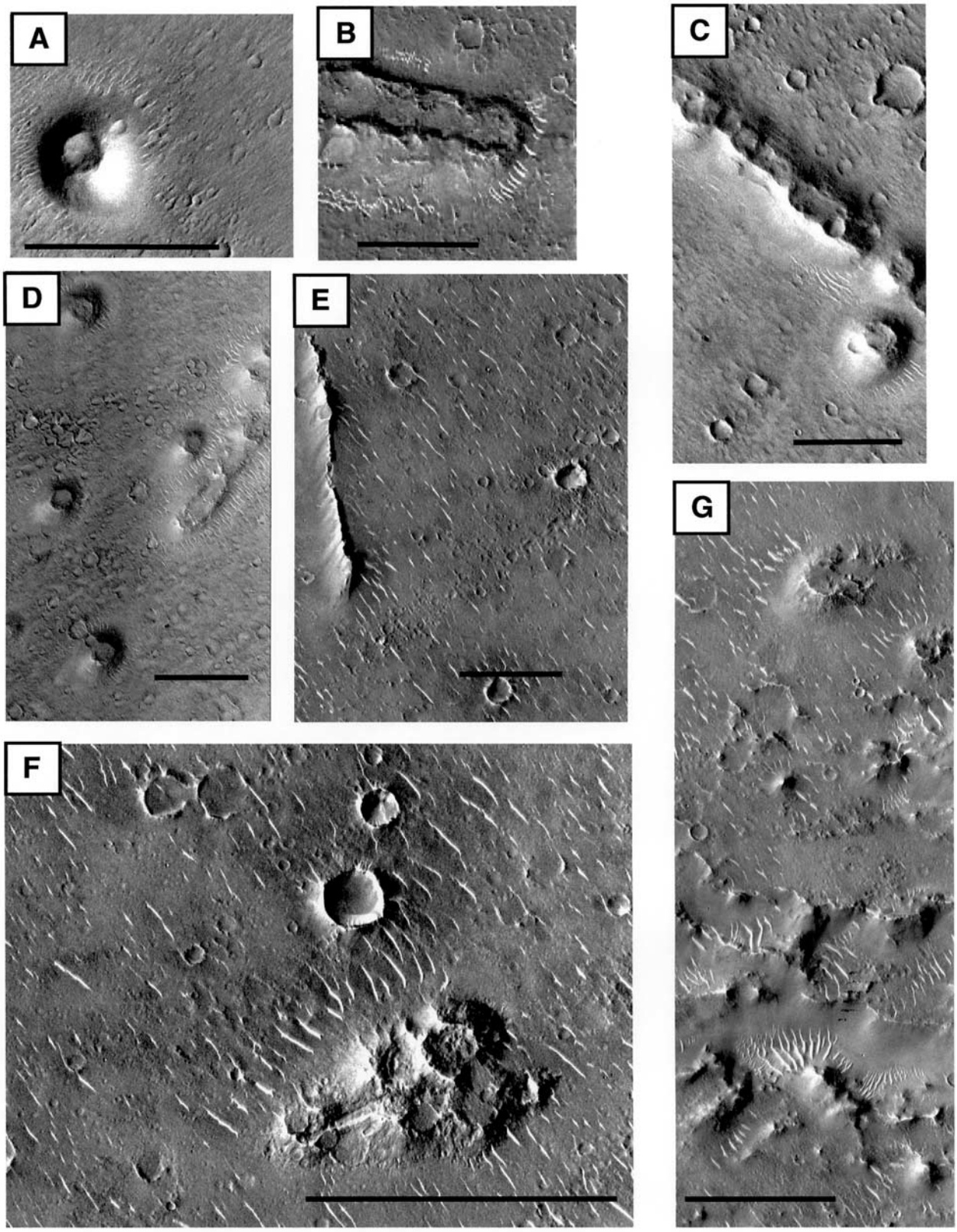
A
B
C
D
E
F
G

with the wrinkle ridges, we compiled a 1/128th degree MOLA DEM of the area directly around the largest subdued ridge and found the average slope to be <2.5°. On the MOLA 1/128th degree DEM (Figure 4c) only impact craters contain slopes which are >2.5° and of sufficient areal extent to show up. Some slopes on the conical hills must exceed this steepness but they are too small to be visible on the MOLA DEM. These slopes are likely to be mainly ≤9–26° (clinometric data from Viking Orbiter images [*Hodges and Moore*, 1994]).

[35] MOLA pulse spread data have been used to derive maps of vertical relief [*Garvin et al.*, 1999; *Smith et al.*, 2001a] and these support the interpretation of the landing region as generally flat (Figure 4d). There are few areas having relief (in RMS units) within MOLA 150 m diameter analysis spots of greater than 4 m. Only the prominent wrinkle ridge and impact craters are clearly seen to have relief of ≤8 m (rms) within the 150 m pulse spots. The 2 m pulse spread (rms) intervals correspond approximately to relief of ~ 10 m within the 150 m spots.

[36] *Head and Bridges* [2001] used a detrended MOLA topographic map of the Isidis basin (Figure 4e) to show the pattern of underlying wrinkle ridges in Isidis. In the outer portions of the inner ring, irregular radial features dominate. Within the innermost 300–400 km the wrinkle ridges display a more isotropic orientation. Superposed on these trends is a general WNW-ESE ridge trend extending through the middle of the basin and across the initial landing ellipses.

[37] The subdued surface expression of the ridges may be a result of resurfacing during both the deposition and erosion that Isidis has undergone since the ridges formed. *Head et al.* [2002] suggested that the underlying wrinkle ridge topography (part of the Hesperian Ridged Plains) of the northern lowlands (including Isidis) had been partially buried by later sediments of the Vastitas Borealis Formation, which includes Hvr [*Tanaka et al.*, 1992]. These sediments may be related to the standing bodies of water proposed by *Parker et al.* [1993] and this is considered as a possible volatile source in the Isidis basin in a later section.

3.4.1. Earth-Based Radar Observations of Isidis Topography

[38] The Goldstone Solar System Radar (GSSR) has performed Earth-based delay-Doppler radar observations of Mars in support of previous landing site selections

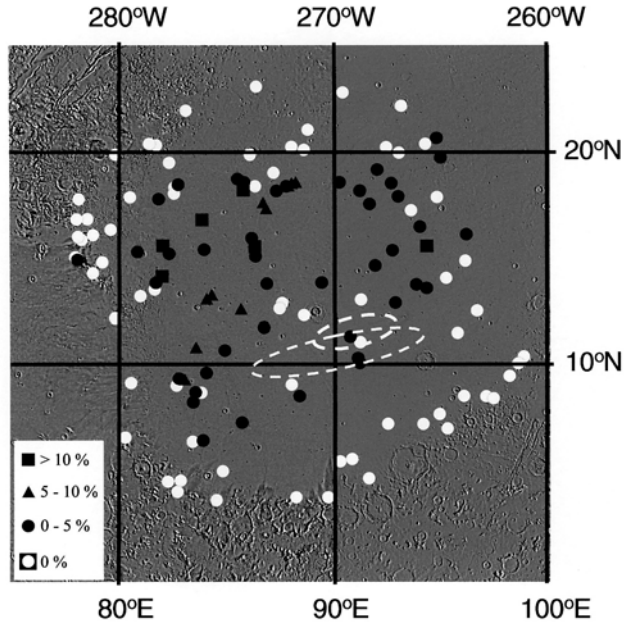

Figure 6. Concentration of conical hills and rings within MOC narrow angle images across Isidis. The highest concentration of these landforms (≤13% of the land surface within some of the images) is present in the western-center of the basin and the lowest is around the margins where many of the images show no cones or rings. The area within the landing ellipses has between 0 and 5% of the area covered by cones and rings.

[e.g., *Haldemann et al.*, 1997]. We have analyzed specular radar echoes at 3.5 cm wavelength (X-band) using the Hagfors model [*Hagfors*, 1964] to obtain Fresnel reflectivity (ρ_0) and RMS slope (θ_{rms}) estimates for "resolution cells" every 0.09° along the radar tracks. The resolution cells are approximately 10 km × 150 km in size. Delay-Doppler radar techniques and analysis are described in several review articles [e.g., *Ostro*, 1993; *Simpson et al.*, 1992]. The processing algorithm used is summarized by *Haldemann et al.* [1997] and is very similar to that used by *Downs et al.* [1975]. This technique probes surface roughness at scales of ten to a hundred radar wavelengths and so

Figure 5. (opposite) MOC narrow angle images (north is at top) within Isidis. (a) Cone (we suggest a tuff cone), as found across the Isidis basin (MOC ab103405, 16.8°N, 276.0°W, 1 km scale, 2.95 m pixel resolution). See text for discussion of cones' origin. Linear, transverse dunes are also visible as bright albedo features around the cone. (b) Eroded conical landform. This remnant of a cone or joined cones has been eroded, showing gullying on its slopes (MOC m1300766, 8.7°N, 271.6°W, 1 km scale, 5.89 m pixel resolution). (c) Typical chain of interlinked cones or rings (MOC ab103405, 16.8°N, 276.0°W, 1 km scale). (d) Isolated cones and a chain of possible tuff rings in the west of the image. Linear, transverse dunes are also clear around the tuff rings (M0901055, 12.7°N, 274.3°W, 1 km scale, 2.95 m pixel resolution). (e) Typical land surface in the landing region, showing a generally flat, cratered plain. The most prominent feature in this image is the 2 km long, N-S ridge. The sharply defined and narrow topography give it the appearance of an igneous intrusion (M0302859, 10.4°N, 268.9°W, 1 km scale, 1.76 m pixel resolution). (f) This image is a different part of the MOC image in Figure 5e and shows degraded tuff cones, the slopes having signs of gullying and mass wasting. The coexistence of the cones across Isidis in differing degrees of erosion suggests that they formed (in both fracture-controlled chains and singly) over a wide period of time. (g) This MOC image contains the roughest terrain identified within the MOC images (a few km^2 and too small an area to show up in our MOLA DEM, Figure 4). The ridges (arrowed) may include the surface exposure of igneous intrusions, although displacement by faults creating scarps may also have occurred. MOC m0202490, 10.2°N, 268.8°W, 1 km scale, 1.76 m scaled resolution. Images from NASA/JPL/Malin Space Science Systems/USGS. There are currently 40 images across the landing area.

provides information on a finer scale (i.e. decimeter to meter scales) than is available from MOLA.

[39] While no radar tracks in the GSSR database directly sample the Beagle 2 landing site, there are six tracks that sample the various geologic units in the Isidis basin, and in particular Hvr. The Isidis track coverage is given in Table 3. We have calculated the statistics of the radar model fits for all the data between 261° and 281°W, and between 2° and 22°N. The means and standard deviations of the Hagfors model fits are listed in Table 3. For comparison we also list the average values for the units near the Mars Pathfinder landing site and the average value for the resolution cells containing that lander. The Hvr and Aps units which fill the center of the Isidis basin are both sufficiently reflective for the Beagle 2 radar altimeter to operate during entry. These two units also have the lowest θ_{rms} values of the units around the basin ($2.4° \pm 0.9°$ and $3.2° \pm 1.3°$ respectively; Tables 2 and 3) and are smoother than the Pathfinder landing site ($5.4° \pm 1.1°$).

[40] The radar results suggest that at the decimeter to meter scale Isidis is smoother than the Pathfinder landing site. This is consistent with the predicted lower average rock abundances of Isidis compared to those encountered at Ares Vallis and is beneficial for a safe landing.

3.5. Conical Landforms and Possible Magma-Ice Interaction

[41] Conical landforms are a characteristic feature of the Isidis land surface and they have received a lot of attention since they were identified in Viking images [e.g., *Grizzaffi and Schultz*, 1989; *Frey and Jarosewich*, 1982]. Subkilometer diameter cones with summit pits are found singly, in clusters or (specific to the Isidis basin) along chains which can reach over 20 km in length throughout Isidis [*Hodges and Moore*, 1994]. Working from Viking Orbiter images, *Grizzaffi and Schultz* measured the orientation of cone chains around the outer part of the Inner Plains Deposits (shown in Figure 3a). The long arcuate arrangement of many of the cones [*Frey and Jarosewich*, 1982] implies some structural or stress-related control on the distribution of the cones, although whether this is related to the orientations of underlying wrinkle ridges or overall structure of the basin is not clear.

[42] Our study shows that the morphology of the cones varies, irrespective of whether they occur singly or in chains (Figures 5a–5d). Some have a relatively shallow saucer-like summit depression and look like terrestrial cinder cones, except for the crucial absence of associated lava flows (this is discussed further in the next subsection). Others, with larger and deeper summit depressions, have the appearance of elevated rings rather than cones, and resemble terrestrial tuff cones and tuff rings.

[43] The elevated and sometimes elliptical nature of these rings distinguishes them from impact craters. In addition to the range of heights and shapes shown by the cones and rings, these landforms exhibit a variety of erosional states, from relatively fresh-looking, through to highly eroded, with the sides of the cones sometimes showing signs of degradation (Figures 5b and 5f). The variation in erosional state also suggests that the cones formed over a long period of time and the fresh appearance of some of them requires that at least some postdate the underlying lavas of the Hesperian Ridged Plains.

[44] Inspection of the MOC images within the landing region also reveals that the cones or elevated rings can cover up to ~13% of the surface, with the higher proportions generally being found in the western-central part of the basin (Figure 6). The lowest areal coverage of cones occurs around the margin of the basin floor and most of the MOC images in this area show no cones.

[45] Proposed mechanisms for the cones' formation have included explosive volcanism resulting in cinder cones [*Plescia*, 1980], phreatomagmatic explosions forming pseudocraters [*Frey and Jarosewich*, 1982], and overpressure in volatile-rich sediments causing mud volcanism [*Ori et al.*, 2001; *Tanaka et al.*, 2000; *Hoffman et al.*, 2001]. The Isidis cones have similar crater/cone diameter ratios (0.45–0.54) to Icelandic pseudocraters which formed through the explosive contact of lava with ice or water-rich ground [*Frey and Jarosewich*, 1982; *Hodges and Moore*, 1994], but given the lower Martian surface gravity and atmospheric pressure pseudocraters may be systematically broader and flatter than on the Earth and higher crater-cone diameter ratios than those of terrestrial examples would be expected [*Wilson and Head*, 1994; *Fagents and Wilson*, 1996].

[46] Our examination of higher resolution MOC images of the cones rules out other models involving glacial origins or ablation of glacial debris [*Grizzaffi and Schultz*, 1989] as their distinct summit craters strongly suggest an explosive origin. However, there is no sign of an association with lava flows, as is the case in terrestrial pseudocraters and the more obviously pseudocrater-like cones in Amazonis and surrounding regions [*Lanagan et al.*, 2001]. As pointed out by *Hoffman et al.* [2001] there appears to be no evidence of breached cones or associated lava flows to support the suggestion that they are cinder cone volcanoes. Mud volcanism would require the deposition of volatile-rich sediments, for which there is some evidence [*Grizzaffi and Schultz*, 1989; *Tanaka et al.*, 2000], although there is no clear evidence whether the depth and speed of deposition would have been adequate to form mud volcanoes. On Earth, mud volcanism is associated with km-thick sediment accumulations in tectonically active areas [*Milkov*, 2000] with resultant development of over-pressuring. In Isidis the thickness of deposits is likely to be no more than a few hundred meters at most because the low elevation of the basin (−3.6 to −3.9 km) and the surface expression of the basement wrinkle ridges does not allow for km-thick accumulations of sediment. It is, therefore, difficult to explain the cones as pseudocraters or mud volcanoes.

3.5.1. Cinder Cones or Tuff Cones?

[47] Evidence supporting a link between the cones and igneous activity is present in some features on the basin surface which appear to be surface exposures of exhumed dykes (Figures 5e and 5g). Figure 5g also shows the roughest region identified within our landing ellipse from MOC or MOLA data. The scarps (arrowed) may be intrusions. Intrusions could have acted as melt conduits for the cones and rings. The exhumation of dykes is also consistent with the substantial erosion of the Isidis land surface. Assuming an igneous origin, the cones in Isidis might be either cinder cones [*Plescia*, 1980] or tuff cones [*Hodges and Moore*, 1994]. We consider both possibilities.

[48] Cinder cones are produced by the explosive exsolution of magmatic gas, leading to fragmentation of the

magma, during magma ascent, resulting in the eruption and proximal deposition of fragmented pyroclasts [e.g., *Head and Wilson*, 1987, 1989]. On Earth, many cinder cones are accompanied by lava flows that escape through a lateral breach in the conduit during the later stages of the eruption [*Wood*, 1980]. Furthermore, pyroclasts may strike the ground at a sufficient rate and temperature to supply a rootless (clastogenic) lava flow.

[49] As pointed out by *Hoffman et al.* [2001] there appears to be no evidence of breached cones or associated lava flows to support the suggestion that the Isidis cones are cinder cones. However, comparison between the Isidis cones and terrestrial examples is complicated by the fact that the lower Martian atmospheric pressure would result in significantly greater fragmentation of erupting magmas under cinder cone conditions. Current modeling [*Mitchell et al.*, 2002] suggests that exsolution and expansion of relatively small quantities of magmatic volatiles (less than 0.1 wt%) during Martian basaltic volcanic eruptions can result in highly explosive eruptions, more typical of those associated with volatile rich (~6 wt% water) rhyolitic magmas on Earth. Moreover, significantly smaller (by a factor of ~100 [*Wilson and Head*, 1994]) clast sizes would be generated, leading to increased temperature losses due to adiabatic expansion and radiative and convective heat loss in flight. Hence it is plausible that, for vertical or near-vertical conduits (in which magma and volatiles would be well-coupled), the low atmospheric pressure of Mars could cause sufficient near-vent fragmentation to preclude the formation of lava flows, so despite the absence of identified lava flows in association with the Isidis cones, a cinder cone origin remains possible.

[50] However the other, perhaps more likely origin, is through phreatomagmatic eruptions building tuff cones and tuff rings. These form on Earth when a explosive eruption is driven by steam generated from the entrainment of ambient water, with water/magma volume ratios of about 1:1 for tuff rings [*Lorenz*, 1986; *Wohletz and McQueen*, 1984] and up to about 10:1 for tuff cones [*Wohletz and Sheridan*, 1983; *Vesperman and Schmincke*, 2000]. The distinction between tuff cones and tuff rings may be largely attributable to a variety of eruption conditions, but both require the involvement of locally entrained volatiles [*Sohn*, 1996]. The involvement of ambient water leads to lower ejecta emplacement temperatures than for cinder cones, and so tuff cones or rings are rarely associated with effusive lava flow activity, which is consistent with our observations of Isidis.

[51] Terrestrial tuff cones typically have slopes of 10–30°, heights varying from 50–370 m and diameters of up to 1.5 km [*Vesperman and Schmincke*, 2000]. In a photoclinometric study of the Isidis cones, *Hodges and Moore* [1994] gave typical profiles and dimensions with heights of 30–100 m and slopes of approximately 9–26°. The slightly lower slopes of the Isidis cones are consistent with trends expected with such eruptions under Martian conditions [e.g., *Wilson and Head*, 1994].

[52] Both magmatic and phreatomagmatic activity seem plausible for the formation of the Isidis cones. Therefore we tend to favor a tuff cone, rather than cinder cone, interpretation because there is independent evidence for the volatile-rich substrate in the ejecta patterns of some of the Isidis larger impact craters, and the high water-magma ratios

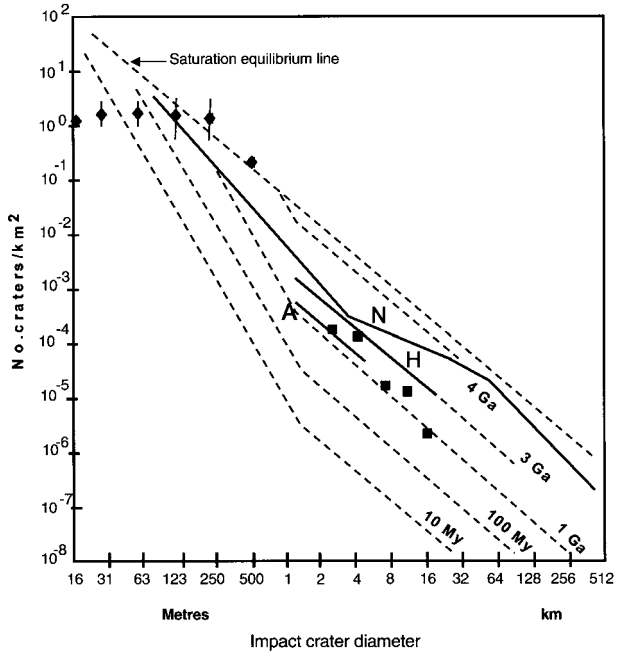

Figure 7. Crater count within Inner Plains of Isidis basin. Diamonds are crater counts taken from 3 narrow angle MOC images (M0903399, M2001670, M0202490), squares crater counts on MDIM photomosaic. A Amazonian, H Hesperian, N Noachian isochrons. Saturation Equilibrium Line is the line showing maximum possible crater densities, i.e., addition of new impact structures obliterates older ones rather than increasing the crater density seen in images. The crater density of smaller craters <120 m diameter cuts across the isochrons as a result of crater infilling by aeolian deposition or erosion. Diagram from *Hartmann and Neukum* [2001]. Vertical bars are ±2 sd errors, where calculated.

associated with tuff activity would be sufficient to suppress the formation of all lava flows.

3.5.2. Isidis Volatile Sources

[53] Terrestrial tuff cones and rings are associated with eruptions under standing water or through water-saturated rocks and soil [*Head and Wilson*, 2002]. On Mars, either H_2O or CO_2 ice could provide suitable volatile reservoirs for this process. The variable ages of the cones suggest that there must have been recharge of the volatiles within the subsurface between episodes of eruption. This could be related to the influx of sediments over the basin floor from the surrounding highlands or to recharge from the atmosphere possibly via obliquity-controlled climate changes as suggested by *Mellon and Jakosky* [1995].

[54] Another possibility for the origin of volatiles associated with the formation of tuff cones is the presence of standing bodies of water in Isidis. It is clear from the dimensions of the outwash channels which lead into the northern plains that the associated floods could have left extensive lakes and possibly oceans [e.g., *Head et al.*, 2001]. *Parker et al.* [1993] identified two possibly shorelines along the margins of the northern plains including Isidis. These shorelines have not been recognized in MOC images [*Malin and Edgett*, 2000]. However, *Head et al.* [1999] used MOLA data to show that one of the shorelines ("contact 2"), which

lay at −3760 m, was within 60 m elevation of all the major outwash channel terminations. This contact lies within the Isidis inner plains and encloses the Beagle 2 landing ellipses. If an ocean or oceans did exist, it is uncertain whether the timing and duration or these events are consistent with the range of ages of the Isidis cones.

[55] The Beagle 2 Lander may be able to provide more information about the Isidis cones and the associated volatile activity that we presume occurred. For instance the camera might view some of the cones and, through Beagle's mineralogical and mass spectrometer analyses, an indication may be obtained of whether H_2O or CO_2 ice is present in the subsurface. Identification of substantial quantities of carbonate minerals would also suggest ancient fluids had high proportions of CO_2, whereas a much higher abundance of sheet silicates compared to carbonate would be consistent with water-dominated fluids.

3.6. Dune and Aeolian Features

[56] Areas surrounding the conical landforms in Isidis often contain high-albedo transverse dunes, with a typical spacing of 50–100 m. Dunes are generally oriented NW-SE and dunes are often concentrated near the SE and NW ends of cone ridges and in the gaps within ridges consistent with the surface wind-strength having been intensified in those places because of the obstruction to airflow caused by the cones. (Figure 5). In the General Circulation Model (GCM) of *Greeley et al.* [1993] the prevalent wind direction during northern hemisphere autumn and winter when the surface wind stress is greatest comes from the NE. However, we have not yet found any firm indication in the Isidis MOC images to indicate whether the dune-forming wind direction is mainly from the NE or the SW. In addition to their GCM, *Greeley et al.* [1993] showed that some bright streak directions on Viking images of Isidis indicated a prevalent wind direction from SW to NE. Therefore, if there is a single prevalent wind direction associate with dune formation in the area of our landing site then it remains unclear.

[57] Similar dunes are also found in the interiors of some of the impact craters, and bright NW-SE streaks in the lee of some cones and impact craters may indicate local accumulations of dust. Dune length (typically reaching at least 100 m) shows that they are larger landforms than the meter-sized drifts which were seen at the Viking and Pathfinder landing sites. Smaller drifts such as those are probably too small to be visible in the Isidis MOC images. However, the similar albedos of Isidis and the previous landing sites suggests that the Beagle 2 site will also have dust and drift partially covering the surface rocks and in small accumulations. Martian sand dunes may have a width:height ratio of 10:1 [*Breed et al.*, 1979], and on this basis the Isidis sand dunes seen in the MOC images are expected to be typically up to a few meters in height. Only exceptionally on Mars do dunes reach heights up to 150 m [*Breed et al.*, 1979].

[58] Isidis is not a frequent center for major, localized dust storm activity. In a survey of 120 regional dust storms observed between 1894 and 1984, *Martin and Zurek* [1993] listed 2 of them as being centered on Isidis.

3.7. Impact Craters and Resurfacing of the Isidis Basin

[59] We conducted some counts on impact craters <1 km diameter seen in three of the MOC narrow angle images within the landing ellipse, with the aim of identifying any episodes of erosion or deposition within Isidis. Counts of larger craters were performed on MDIM1 images. One of the MOC counts was performed on the west side of the initial landing ellipses (Hesperian Ridged Plains Hvr) and the other two on the eastern side (Figure 2; mapped as Amazonian Smooth Plains, Aps by *Greeley and Guest* [1987]). The final landing ellipse lies within Aps. The average results are plotted on Figure 7. These counts and the plotted average show that the expected production functions for unaltered terrains [*Hartmann and Neukum*, 2001] have not been preserved in Isidis for the smallest craters (<120 m). The most obvious agent for this process of crater degradation is the aeolian action described in the previous section. However, some large 15–20 km, partially buried "ghost" craters in the Amazonian Smooth Plains formation (Figures 2 and 4a) may have resulted either from the Amazonian influx of lava or sediment across the basin, or, through erosion of the Isidis land surface that has affected many of the cones. The MOC evidence for erosion is, as stated previously, the degraded and gullied state of some of the cones and exhumation of a dyke-like feature.

[60] The area covering the three most prominent partially buried craters (Figure 2) is also part of the area with a relatively high bulk TI (Figure 3a) which is consistent with an influx of sediment from the Libya Montes region of the highlands across the basin floor and over some of the crater rims. There is no evidence for a higher proportion of the conical hills in this part of the basin, the Aps outcrop and high TI margin to the basin have the lowest proportion of cones, mainly <5% by area of the MOC images. There is therefore no obvious link between the inferred predominant direction of sediment influx over Isidis as shown by the TI pattern and the formation of the conical landforms. This is consistent with a volcanic rather than sedimentary origin for the cones.

[61] One of the larger impact craters (25 km diameter) within Isidis is located to the NE of the landing ellipses at 12.5°N, 271°W. It is surrounded by a well-defined lobate ejecta pattern of up to 15 km width. Such ejecta patterns, which are common across the northern plains, may indicate impact into an ice-rich substrate [*Carr*, 1981]. The largest crater in the Inner Plains deposits near the landing ellipses is the 60 km diameter impact crater at 10°N, 266°W. It is likely that some of the rocks on the ground surface within the landing ellipses originated as impact ejecta from this crater. If it is assumed that ejecta travel 2.0 times the radii of impact craters within Isidis [*Mouginis-Mark*, 1979] then the ejecta from the 60 km diameter impact crater at 10°N, 266°W is likely to have reached 60 km from the crater rim and cover approximately 450 km^2 of the NE corner of the initial landing ellipse for a flight path angle of 15° (Figure 4b). The area within the larger, initial three sigma landing ellipses also contains 9 craters ≥3 km diameter (∼90 km^2). There are 2 such impact craters within the smaller final landing ellipse.

4. Implications for the Nature of the Isidis Landing Site

[62] MOLA and MOC data from Mars Global Surveyor have provided evidence that extensive volcanism has taken

place within the northern plains during the Hesperian epochs, into the late Amazonian epochs, and locally to within the last few tens of Ma [*Hartmann and Berman*, 2000]. It is reasonable to suppose that this has affected Isidis and is associated with the formation of the conical hills and the intrusion of occasionally visible dykes. The chains of conical hills and rings, together with dykes which may have acted as magma conduits, could be related to the underlying structural and fault patterns within the basin. On the basis of the current evidence (particularly the absence of lava flows) we favor an origin as tuff cones and tuff rings through phreatomagmatic activity (although we recognize that an origin as cinder cones cannot be ruled out).

[63] The variable state of erosion of the presumed tuff cones shows that they formed intermittently over a long part of the Martian geological record. As tuff cones require substantial fluid reservoirs for explosive magma-volatile interaction to take place (i.e. probably water ice or CO_2 ice accumulations) their presence in a variety of degradational states suggests that Isidis had substantial near-surface ice over much of the Amazonian and perhaps Hesperian. This volatile reservoir must have been recharged at various times, possibly during sediment influx over the basin from the surrounding highlands, or, alternatively, from recharge via the atmosphere.

[64] The pattern of thermal inertia across the basin suggests that the predominant sediment influx was from the Noachian terrain around the southern and eastern margins of the basin. The ground has undergone some resurfacing probably as a result of aeolian activity. In particular this is shown by the eroded nature of some of the conical hills and the degradation or infilling of small, <120 m diameter, impact craters. The partial infilling of some larger km-size craters is probably a result of the Amazonian influx across the basin's underlying Hesperian volcanic basement. Signs of aeolian activity may be visible from the Beagle Lander in the form of dust drifts and more occasional sand dunes $\leq$10 m high. The predicted proportion of rocks >0.10 m diameter (mean 11% across the landing ellipses, 0–15% within the final ellipse) is less than that of the Viking 1,2 and Pathfinder sites which had predicted rock abundances of 15%, 18% and 18% [*Golombek et al.*, 1997a], with similar values observed at the landing sites (e.g., 16% at the Pathfinder site [*Pathfinder Rover Team*, 1997; *Moore and Keller*, 1990, 1991]).

[65] The similarity of albedos and spectral characteristics of Isidis and the previous landing sites suggest that Beagle 2 will encounter an oxidized surface with a partial covering of sulfur-rich dust, although the high fine component TI values suggest more extensive coverage by oxidized duricrusts than was encountered by the other landers. MOLA show that Isidis is a flat basin with subdued topography and relatively few slopes greater than a few degrees and so the panoramic view from the Beagle 2 Lander is likely to show a terrain that is generally as flat as that encountered by the previous landers. Radar data show that the site is also smooth at decimeter to meter scales.

[66] An important difference is that Isidis contains evidence in the form of volcanic cones and rings for prolonged subsurface volatile activity. This is likely to be reflected in the mineralogy encountered, for instance a high proportion of clays, sulfates, perhaps carbonates and other secondary minerals resulting from the alteration of the bedrock. If the cones are tuff cones (derived from lava/ice interaction), then this suggests that there was a near-surface H_2O or CO_2 ice reservoir underlying Isidis during Hesperian to Amazonian times which was periodically recharged. However, current near-surface major ice reservoirs are situated in midlatitude regions [*Mustard et al.*, 2001] and only slightly deeper reservoirs are likely to be present in Isidis.

4.1. Exobiological Potential of Isidis

[67] The pattern of thermal inertia indicates that much of the sediment which spread over the Isidis basin was derived from the Noachian terrain to the south. It is within Noachian sequences that meter-scale layered sedimentary rocks may be present [e.g., *Malin and Edgett*, 2000] acting as a trap for part of the CO_2 which was present in the thicker early atmosphere. *Bridges et al.* [2001] suggested on the basis of carbonate concentrations in Martian meteorites that the equivalent of 50–250 mbar pCO_2 could have been trapped in the upper Martian crust. Sampling such material, present as rocks (average 11% coverage in the landing ellipse) transported onto the surface of the Isidis basin from the surrounding highlands, could provide an important insight into the early geology and atmosphere of Mars and is one of the obvious ways to search for traces of any past life. Although the surface rocks at the Viking 1,2 and Pathfinder outflow channel sites are generally regarded as basaltic or basaltic andesite in origin [*Bell et al.*, 2000], the larger the number of sample localities reached by probes at Isidis and other landing sites, the greater the chance that any sedimentary rocks will be encountered.

[68] As argued above it is likely that Isidis has a higher proportion of its surface covered by duricrust than Pathfinder or Viking 1 and 2. Duricrusts might have originated through direct evaporation of standing water at some time in the basin's history e.g., the Hesperian. Alternatively they may be associated with the sediment influx across the basin. They could also have formed as a result of ice sublimation in geologically recent times. Sublimation of ice to vapor takes place during the Mars spring and summer. This process could act to concentrate salts and volatiles within the top few meters of the ground [*Mustard et al.*, 2001].

[69] The igneous or explosive volatile activity centered within the Isidis basin over much of its history is a potential source of the energy and water necessary for life to have existed. Subsurface hydrothermal systems are considered one of the geological environments on Mars at which life may have existed [e.g., *Jakosky and Mellon*, 2001; *Farmer and Des Marais*, 1999] and Isidis may have preserved traces of ice/fluid reservoirs and hydrothermal (H_2O-CO_2) systems. The variable state of erosion of the cones in Isidis indicates that such hydrothermal systems could have existed over a protracted period of time (e.g., throughout the Amazonian). The explosive activity that formed the cones and rings would have excavated material from such systems onto the surface. These arguments suggest that the Beagle 2 landing site has a good exobiological potential for an area whose selection was so tightly constrained by engineering considerations. At a minimum there will almost certainly be abundant material such as the duricrust and soil and dust that has experienced interactions between volatiles in the atmosphere and subsurface, and this environment may have

trapped more complex organic molecules. The sampling techniques of Beagle, including being able to burrow into the soil and underneath rocks enhance the potential for locating preserved organic material beneath the highly oxidized top surface [e.g., *Clark*, 1998] which the Viking Landers might have missed.

[70] **Acknowledgments.** JCB and KLM are funded by PPARC. AMS is funded by a PPARC studentship. MRS acknowledges joint funding for his post from the UK Royal Society Industrial Fellowship scheme and the University of Leicester. JWH acknowledges support from a NASA Mars Data Analysis Program grant. MPG and AFCH were supported by the National Aeronautics and Space Administration, Mars Data Analysis Program at the Jet Propulsion Laboratory, California Institute of Technology. SRL acknowledges support from ESA under ESTEC contract 11369/95/NL/JG(SC) for the development of the Mars Climate Database. Jim Garvin is thanked for providing the MOLA pulse spread map (Figure 4d) and Phil Christensen is thanked for providing an integrated IRTM data set as well as TES albedo data. The assistance of Dr David E. Smith, GSFC for early release of MOLA data in the initial stages of this study is appreciated. The authors wish to thank Michael Mellon and an anonymous reviewer for their comments.

References

Aharonson, A., M. T. Zuber, and D. H. Rothman, Statistics of Mars' topography from the Mars Orbiter Laser Altimeter: Slopes, correlations, and physical models, *J. Geophys. Res.*, *106*, 23,723–23,736, 2001.

Bandfield, J. L., V. E. Hamilton, and P. R. Christensen, A global view of Martian surface compositions from MGS-TES, *Science*, *287*, 1626–1630, 2000.

Bell, J. F., III, et al., Maneralogic and compositional properties of Martian soil and dust: Results from Mars Pathfinder, *J. Geophys. Res.*, *105*, 1721–1755, 2000.

Breed, C. S., M. J. Grolier, and J. F. McCauley, Morphology and distribution of common "sand" dunes on Mars: Comparison with the Earth, *J. Geophys. Res.*, *84*, 8183–8205, 1979.

Bridges, J. C., D. C. Catling, J. M. Saxton, T. D. Swindle, I. C. Lyon, and M. M. Grady, Alteration assemblages in Martian meteorites: Implications for near-surface processes, in *Evolution of Mars*, edited by R. Kallenbach, J. Geiss, and W. K. Hartmann, pp. 365–392, Kluwer Acad., Norwell, Mass., 2001.

Carr, M. H., *The Surface of Mars*, 232 pp., Yale Univ. Press, New Haven, Conn., 1981.

Chicarro, A. F., P. H. Schultz, and P. Masson, Global and regional ridge patterns on Mars, *Icarus*, *50*, 129–139, 1985.

Christensen, P. R., The spatial distribution of rocks on Mars, *Icarus*, *68*, 217–238, 1986.

Christensen, P. R., and H. J. Moore, The Martian surface layer, in *Mars*, edited by H. H. Kieffer et al., pp. 1–33, Univ. of Ariz. Press, Tucson, 1992.

Christensen, P. R., et al., Detection of crystalline hematite mineralization on Mars by the Thermal Emission Spectrometer: Evidence for near-surface water, *J. Geophys. Res.*, *105*, 9623–9642, 2000.

Clark, B. C., Surviving the limits to life at the surface of Mars, *J. Geophys. Res.*, *103*, 28,545–28,555, 1998.

Downs, G. S., P. E. Reichley, and R. R. Green, Radar measurements of Martian topography and surface properties: The 1971 and 1973 oppositions, *Icarus*, *26*, 273–312, 1975.

Fagents, S. A., and L. Wilson, Numerical modelling of ejecta dispersal from transient volcanic explosions on Mars, *Icarus*, *123*, 284–295, 1996.

Farmer, J. D., and D. J. Des Marais, Exploring for a record of ancient Martian life, *J. Geophys. Res.*, *104*, 26,977–26,995, 1999.

Frey, H., and M. Jarosewich, Subkilometer Martian volcanoes: Properties and possible terrestrial analogs, *J. Geophys. Res.*, *87*, 9867–9878, 1982.

Frey, H., J. Roark, and S. Sakimoto, Detailed topographic structure of the Isidis Impact Basin from MOLA data (abstract), *Lunar Planet. Sci.* [CD-ROM], *XXX1*, 1748, 2000.

Frey, H. V., K. M. Schockey, E. L. Frey, J. H. Roark, and S. A. H. Sakimoto, A very large population of likely buried impact basins in the northern lowlands of Mars revealed by MOLA data, *Lunar Planet. Sci.*, *XXXII*, 1860, 2001.

Garvin, J. B., J. J. Frawley, and J. B. Abshire, Vertical roughness of Mars from the Mars Orbiter Laser Altimeter, *Geophys. Res. Lett.*, *26*, 381–384, 1999.

Golombek, M. P., and D. Rapp, Size-frequency distributions of rocks on Mars and Earth analog sites: Implications for future landed missions, *J. Geophys. Res.*, *102*, 4117–4129, 1997.

Golombek, M. P., R. A. Cook, H. J. Moore, and T. J. Parker, Selection of the Mars Pathfinder site, *J. Geophys. Res.*, *102*, 3967–3988, 1997a.

Golombek, M. P., et al., Overview of the Mars Pathfinder mission and assessment of landing site predictions, *Science*, *278*, 1743–1748, 1997b.

Golombek, M. P., H. J. Moore, A. F. C. Haldemann, T. J. Parker, and J. T. Schofield, Assessment of Mars Pathfinder landing site predictions, *J. Geophys. Res.*, *104*, 8585–8594, 1999.

Golombek, M. P., B. M. Jakosky, and M. T. Mellon, Thermal inertia of rocks and rock populations (abstract), *Lunar Planet. Sci.* [CD-ROM], *XXX11*, 1115, 2001.

Greeley, R., and J. E. Guest, Geologic map of the eastern equatorial region of Mars, *U.S. Geol. Surv. Misc. Invest. Ser.*, *Map I 1802B*, 1987.

Greeley, R., A. Skypeck, and J. B. Pollack, Martian aeolian features and deposits: Comparisons with general circulation model results, *J. Geophys. Res.*, *98*, 3183–3196, 1993.

Grizzaffi, P., and P. H. Schultz, Isidis Basin: Site of ancient volatile-rich debris layer, *Icarus*, *77*, 358–381, 1989.

Hagfors, T., Backscattering from an undulating surface with applications to radar returns from the Moon, *J. Geophys. Res.*, *69*(18), 3779–3784, 1964.

Haldemann, A. F. C., D. L. Mitchell, R. F. Jurgens, M. A. Slade, and D. O. Muhleman, Mars Pathfinder landing site assessment with Goldstone delay-Doppler and CW radar experiments, *J. Geophys. Res.*, *102*, 4097–4106, 1997.

Hartmann, W. K., and D. C. Berman, Elysium Planitia lava flows: Crater count chronology and geological implications, *J. Geophys. Res.*, *105*, 15,011–15,025, 2000.

Hartmann, W. K, and G. Neukum, Cratering chronology and the evolution of Mars, in *Evolution of Mars*, edited by R. Kallenbach, J. Geiss, and W. K. Hartmann, pp. 165–194, Kluwer Acad., Norwell, Mass., 2001.

Head, J. W., and J. C. Bridges, Beagle 2 landing site: Regional characteristics of Isidis Planitia from MOLA data (abstract), *Lunar Planet. Sci.* [CD-ROM], *XXXII*, 1236, 2001.

Head, J. W., and L. Wilson, Lava fountain heights at Pu'u O'o, Kilauea, Hawaii: Indicators of amount and variations of exsolved magma volatiles, *J. Geophys. Res.*, *92*, 13,715–13,719, 1987.

Head, J. W., and L. Wilson, Basaltic pyroclastic eruptions: Influence of gas-release patterns and volume fluxes on fountain structure and the formation of cinder cones, spatter cones, rootless flows, lava ponds and lava flows, *J. Volcanol. Geotherm. Res.*, *37*, 261–271, 1989.

Head, J. W., and L. Wilson, Mars: General environments and geologic settings of magma/H_2O interactions, in *Volcano-Ice Interaction on Earth and Mars*, *Geol. Soc. Spec. Publ.*, in press, 2002.

Head, J. W., III, H. Hiesinger, M. A. Ivanov, M. A. Kreslavsky, S. Pratt, and B. J. Thomson, Possible oceans on Mars: Evidence from Mars Orbiter Laser Altimeter data, *Science*, *286*, 2134–2137, 1999.

Head, J. W., R. Greeley, M. P. Golombek, W. K. Hartmann, E. Hauber, R. Jaumann, P. Masson, G. Neukum, L. E. Nyquist, and M. H. Carr, Geological processes and evolution, in *Evolution of Mars*, edited by R. Kallenbach, J. Geiss, and W. K. Hartmann, pp. 263–292, Kluwer Acad., Norwell, Mass., 2001.

Head, J. W., III, M. A. Kreslavsky, and S. Pratt, Northern lowlands of Mars: Evidence for widespread volcanic flooding and tectonic deformation in the Hesperian period, *J. Geophys. Res.*, *107*, 31–59, 2002.

Hodges, C. A., and H. J. Moore, *Atlas of Volcanic Landforms on Mars*, 194 pp., *U.S. Geol. Surv. Prof. Pap.*, 16–1534, 1994.

Hoffman, N., J. S. Kargel, and K. L. Tanaka, Isidis Basin-A potential focus of cryovolcanic activity on Mars (abstract), *Lunar Planet. Sci.* [CD-ROM], *XXX11*, 1493, 2001.

Ivanov, M. A., and J. W. Head, Chryse Planitia, Mars: Topographic configuration from MOLA data and tests for hypothesized lakes and shorelines, *J. Geophys. Res.*, *106*, 3275–3295, 2001.

Jakosky, B. M., and P. R. Christensen, Global duricrust on Mars: Analysis of remote-sensing data, *J. Geophys. Res.*, *91*, 3547–3559, 1986.

Jakosky, B. M., and M. T. Mellon, High-resolution thermal inertia mapping of Mars: Sites of exobiological interest, *J. Geophys. Res.*, *106*, 23,887–23,907, 2001.

Kreslavsky, M. A., and J. W. Head, Kilometer-scale slopes on Mars and their correlation with geologic units: Initial results from Mars Orbiter laser Altimeter (MOLA) data, *J. Geophys. Res.*, *105*, 26,695–26,712, 2000.

Kreslavsky, M. A., and J. W. Head, Fate of outflow channel effluents in the northern lowlands of Mars: The Vastitas Borealis Formation as a sublimation residue from frozen ponded bodies of water, *J. Geophys. Res.*, *107*(E12), 5121, doi:10.1029/2001JE001831, 2002.

Lanagan, P. D., A. S. McEwen, and L. P. Keszthelyi, Rootless cones on Mars indicating the presence of shallow equatorial ground ice in recent times, *Geophys. Res. Lett.*, *28*, 2365–2367, 2001.

Landis, G. A., and P. J. Jenkins, Measurement of the settling rate of atmospheric dust on Mars by the MAE instrument on Mars Pathfinder, *J. Geophys. Res.*, *105*, 1855–1858, 2000.

Lewis, S. R., M. Collins, P. L. Read, F. Forget, F. Hourdin, R. Fournier, C. Hourdin, O. Talagrand, and J.-P. Huot, A climate database for Mars, *J. Geophys. Res.*, *104*, 24,177–24,194, 1999.

Lorenz, V., On the growth of maars and diatremes and its relevance to the formation of tuff rings, *Bull. Volcanol.*, *48*, 265–274, 1986.

Malin, M. C., and K. S. Edgett, Sedimentary rocks of early Mars, *Science*, *290*, 1927–1937, 2000.

Martin, L. J., and R. W. Zurek, An analysis of the history of dust activity on Mars, *J. Geophys. Res.*, *98*, 3221–3246, 1993.

McEwen, A., P. Lanagan, R. Beyer, L. Keszthelyi, and D. Burr, Potential 2003 landing sites in the Cerberus Plains, SE Elysium (abstract), in *First Landing Workshop for MER 2003* [CD-ROM], 9022, Jet Propul. Lab., Pasadena, Calif., 2001.

McGill, G. E., Buried topography of Utopia, Mars: Persistence of a giant impact depression, *J. Geophys. Res.*, *94*, 2753–2759, 1989.

McGill, G. E., and A. M. Dimitrou, Origin of the Martian global dichotomy by crustal thinning in the late Noachian or Early Hesperian, *J. Geophys. Res.*, *95*, 12,595–12,605, 1990.

McSween, H. Y., et al., Chemical, multispectral and textural constraints on the composition and origin of rocks at the Mars Pathfinder landing site, *J. Geophys. Res.*, *104*, 8679–8715, 1999.

Mellon, M. T., and B. M. Jakosky, The distribution and behavior of Martian ground ice during past and present epochs, *J. Geophys. Res.*, *100*, 11,781–11,799, 1995.

Mellon, M. T., B. M. Jakosky, H. H. Kieffer, and P. R. Christensen, High resolution thermal inertia mapping from the Mars Global Surveyor Thermal Emission Spectrometer, *Icarus*, *148*, 355–437, 2000.

Milkov, A. V., Worldwide distribution of submarine volcanoes and associated gas hydrates, *Mar. Geol.*, *167*, 29–42, 2000.

Mitchell, K. L., L. Wilson, and S. J. Lane, Factors limiting the explosivity of volcanic eruptions on Mars, *Lunar Planet. Sci.* [CD-ROM], *XXXIII*, abstract 1766, 2002.

Moore, H. J., and J. M. Keller. Surface material maps of the Viking landing sites on Mars (abstract), in *Reports of Planetary Geology and Geophysics Program-1989*, *NASA Tech. Memo.*, *4210*, 533–535, 1990.

Moore, H. J., and J. M. Keller. Surface material maps of the Viking landing sites on Mars (abstract), in *Reports of Planetary Geology and Geophysics Program-1990*, *NASA Tech. Memo.*, *4300*, 160–162, 1991.

Mouginis-Mark, P. J., Martian fluidized crater morphology: Variations with crater size, latitude, altitude and target material, *J. Geophys. Res.*, *84*, 8011–8022, 1979.

Mustard, F. J., C. D. Cooper, and M. K. Rifkin, Evidence for recent climate change on Mars from the identification of youthful near-surface ground ice, *Nature*, *412*, 411–414, 2001.

Ori, G., G. Komatsu, J. Ormo, and L. Marinangcli, Subsurface models for the formation of mound-like morphologies on Mars (abstract), *Lunar Planet. Sci.* [CD-ROM], *XXXII*, 1539, 2001.

Ostro, S. J., Planetary radar astronomy, *Rev. Mod. Phys.*, *65*(4), 1235–1279, 1993.

Parker, T. J., D. S. Gorseline, R. S. Saunders, D. C. Pieri, and D. M. Schneeberger, Coastal geomorphology of the Martian northern plains, *J. Geophys. Res.*, *98*, 11,061–11,078, 1993.

Pathfinder Rover Team, Characterization of the Martian surface deposits by the Mars Pathfinder Rover, Sojourner, *Science*, *278*, 1765–1768, 1997.

Phillips, R. J., and R. S. Saunders, The isostatic state of Martian topography, *J. Geophys. Res.*, *80*, 2893–2898, 1975.

Plescia, J. B., Cinder cones of Isidis and Elysium, *NASA Tech. Memo.*, *82385*, 263–265, 1980.

Pleskot, L. K., and E. D. Miner, Time variability of Martian bolometric albedo, *Icarus*, *45*, 179–201, 1981.

Sakimoto, S. E. H., H. V. Frey, J. B. Garvin, and J. H. Roark, Topography, roughness, layering, and slope properties of the Medusae Fossae Formation from Mars Orbiter Laser Altimeter (MOLA) and Mars Orbiter Camera (MOC) data, *J. Geophys. Res.*, *104*, 24,141–24,154, 1999.

Schultz, R. A., and H. V. Frey, A new survey of large multi-ringed impact basins on Mars, *J. Geophys. Res.*, *95*, 14,175–14,189, 1990.

Scott, D. H., and K. L. Tanaka, Geologic map of the western equatorial region of Mars, *U.S. Geol. Surv. Misc. Invest. Ser.*, *Map I-1802-A*, 1986.

Simpson, R. A., J. K. Harmon, S. H. Zisk, T. W. Thompson, and D. O. Muhleman, Radar determination of Mars surface properties, in *Mars*, edited by H. H. Kieffer et al., pp. 652–685, Univ. of Ariz. Press, Tucson, 1992.

Sims, M. R., et al., Instrumentation on Beagle 2: The Astro-Biology Lander on ESA's 2003 Mars Express Mission, *Proc. SPIE Int. Soc. Opt. Eng.*, *4137*, 36–47, 2000.

Smith, D. E., and M. T. Zuber, The relationship between MOLA northern hemisphere topography and the 6.1-Mbar atmospheric pressure surface of Mars, *Geophys. Res. Lett.*, *25*, 4397–4400, 1998.

Smith, D. E., W. L. Sjogren, G. L. Tyler, G. Balmino, F. G. Lemoine, and A. S. Konopliv, The gravity field of Mars: Results from Mars Global Surveyor, *Science*, *286*, 94–97, 1999.

Smith, D. E., et al., Mars Orbiter Laser Altimeter (MOLA): Experiment summary after the first year of global mapping of Mars, *J. Geophys. Res.*, *106*, 23,689–23,722, 2001a.

Smith, M. D., J. C. Pearl, B. J. Conrath, and P. R. Christensen, Thermal Emission Spectrometer results: Mars atmospheric thermal structure and aerosol distribution, *J. Geophys. Res.*, *106*, 23,929–23,945, 2001b.

Sohn, Y. K., Hydrovolcanic processes forming basaltic tuff rings and cones on Cheju Island, Korea, *Geol. Soc. Am. Bull.*, *108*, 1199–1211, 1996.

Solomon, S. C., and J. W. Head III, Lunar mascon basins: Lava filling, tectonics and evolution of the lithosphere, *Rev. Geophys.*, *18*, 107–141, 1980.

Tanaka, K. L., D. H. Scott, and R. Greeley, Global stratigraphy, in *Mars*, edited by H. H. Kieffer et al., pp. 345–382, Univ. of Ariz. Press, Tucson, 1992.

Tanaka, K. L., T. Joyal, and A. Wenker, The Isidis Plains unit, Mars: Possible catastrophic origin, tectonic tilting, and sediment loading (abstract), *Lunar Planet. Sci.* [CD-ROM], *XXX1*, 2023, 2000.

Vesperman, D., and H.-U. Schmincke, Scoria cones and tuff rings, in *Encyclopedia of Volcanoes*, edited by H. B. Sigurdsson et al., pp. 683–694, Academic, San Diego, Calif., 2000.

Wilson, L., and J. W. Head, Mars: Review and analysis of volcanic eruption theory and relationships to observed landforms, *Rev. Geophys.*, *32*, 221–263, 1994.

Wohletz, K. H., and R. G. McQueen, Experimental studies of hydromagmatic volcanism, in *Explosive Volcanism: Inception, Evolution, and Hazards, Studies in Geophysics*, pp. 158–169, Natl. Acad. Press, Washington, D. C., 1984.

Wohletz, K. H., and M. F. Sheridan, Hydrovolcanic explosions, II, Evolution of basaltic tuff rings and tuff cones, *Am. J. Sci.*, *283*, 385–414, 1983.

Wood, C. A., Morphometric evolution of cinder cones, *J. Volcanol. Geotherm. Res.*, *7*, 387–413, 1980.

Zimbelmann, J. R., D. A. Crown, J. A. Grant, and D. M. Hooper, The Medusae Fossae Formation, Amazonis Planitia, Mars: Evaluation of proposed hypotheses of origin (abstract), *Lunar Planet. Sci.* [CD-ROM], *XXVII*, 1623, 1997.

Zimbelmann, J. R., D. Hooper, D. Crown, J. Grant, S. Skimoto, and H. Frey, Medusae Fossae Formation: An assessment of possible origins utilizing early results from Mars Global Surveyor (abstract), *Lunar Planet. Sci.* [CD-ROM], *XXX*, 1652, 1999.

Zuber, M. T., et al., Internal structure and early thermal evolution of Mars from Mars Global Surveyor topography and gravity, *Science*, *287*, 1788–1793, 2000.

J. C. Bridges and M. M. Grady, Department of Mineralogy, Natural History Museum, London, UK.

A. M. Seabrook, C. T. Pillinger, and I. P. Wright, PSSRI, Open University, Milton Keynes, UK.

D. A. Rothery, Department of Earth Sciences, Open University, Milton Keynes, UK.

J. R. Kim, J. G. Morley, and J.-P. Muller, Department of Geomatic Engineering, University College London, London, UK.

M. R. Sims, Department of Physics and Astronomy, University of Leicester, Leicester, UK.

T. Duxbury, M. P. Golombek, and A. F. C. Haldemann, Jet Propulsion Laboratory, California Institute of Technology, Pasadena, California, USA.

J. W. Head, Department of Geological Science, Brown University, Providence, Rhode Island, USA.

K. L. Mitchell, Environmental Science Department, Lancaster University, Lancaster, UK.

S. R. Lewis, AOPP, Department of Physics, Oxford University, Oxford OXI 3PU, UK.

C. Moncrieff, Department of Zoology, Natural History Museum, London, UK.